THE
AUSTRALIAN
NATIONAL
UNIVERSITY

RESEARCH SCHOOL OF PHYSICAL SCIENCES

ANU-P/775
JUNE 1980

LIMITS TO EVAPORATION RESIDUE CROSS SECTIONS FROM FISSION AND PARTICLE DECAY AT HIGH ANGULAR MOMENTUM

by

J.O. NEWTON

Department of Nuclear Physics, The Australian National University

Canberra, ACT 2600, Australia

INSTITUTE OF ADVANCED STUDIES

ANU-P/775
JUNE 1980

To be published in Physica Scripta.

LIMITS TO EVAPORATION RESIDUE CROSS SECTIONS FROM FISSION AND PARTICLE DECAY AT HIGH ANGULAR MOMENTUM

J.O. Newton

Department of Nuclear Physics,

Research School of Physical Sciences,

The Australian National University,

Canberra, A.C.T. 2600, Australia.

This was an invited paper given at the

Nobel Symposium on Nuclei at Very High Spin (Sweden)

23-27 June, 1980

Abstract

Limits to evaporation residue cross sections from fission and particle decay at high angular momentum. J.O. Newton (Department of Nuclear Physics, Research School of Physical Sciences, The Australian National University, Canberra, A.C.T. 2600, Australia).

Physica Scripta (Sweden)

The study of γ-rays following heavy-ion induced reactions has provided most of our information regarding nuclear properties at very high angular momentum. The limits set a high angular momentum to the observation of the γ-rays and an alternative possibility for extending our knowledge to still higher angular momenta are considered in this review. A short discussion is given of the limits set by the entrance channel and to the existence of an equilibrated nucleus by the Rotating Liquid Drop Model. Competition between the particle, fission and γ-ray decay modes is described in the framework of the statistical model of the nucleus. Attention is drawn to some of the uncertainties in such analyses and, in particular, to our lack of knowledge of the average squared matrix elements for statistical γ-decay. The necessity to include the important effect of the collective E2 transitions in bands roughly parallel to the yrast line is stressed; this has not normally been done. The limits imposed by α-decay in competition with γ-emission and by higher chance fission are considered. The effect of shell structure and shape changes on decay probabilities and on the recently proposed possibility of observing α-decay from super-deformed nuclei is discussed. It is pointed out that the many open questions can only be solved by very complete and systematic measurements, which hardly exist to date.

1. Introduction

In recent years there has been great interest in nuclear properties at very high angular momentum. The heavy-ion (HI), xnγ reaction and to a lesser extent the (HI, xn, ypγ) reactions, have so far offered the most powerful experimental technique for their study. Measurements on the resolved discrete γ-rays from the decay of yrast or near-yrast states has led to considerable understanding of states with angular momenta up to a little over 20 $\hbar$ and in a few special cases as high as 37 $\hbar$. To investigate nuclei at still higher angular momenta one can study the so called "continuum γ-rays", which cannot be resolved by present techniques because so many pathways are involved. Such studies commenced in the mid 1970s and have given information on nuclear properties up to about 70 $\hbar$. Data are still very sparse because the experiments and their interpretation are both considerably more difficult and laborious than for discrete line measurements. Here I shall consider the factors which determine the upper limits of the angular momenta for which continuum γ-ray studies can be usefully employed and how one may gain information beyond these limits. Although definitive answers cannot at present be given to many of these matters, there is much interesting physics to learn from their study.

A possible upper angular momentum limit to the "existence" of a nucleus is that at which the fission barrier E_f vanishes. For angular momenta in excess of this the nuclear lifetime is of the order of 10^{-21} sec or less. These limiting values ℓ_{II}, estimated from the rotating liquid drop model (RLDM) [1] for typical compound nuclei which can be reached through ^{40}Ar induced reactions, are shown in fig.1. In the region between the curves marked ℓ_I and ℓ_{II} the deformation is expected to increase dramatically, producing so called super-deformed nuclei, which would be of great interest to study. One should appreciate that shell effects may sometimes cause significant

deviations (> 10 ħ) from the RLDM predictions, as shown for example by Faber et al.[2]. Also the liquid drop fission barriers may be somewhat too high for A ≲ 200 due to neglect of the finite range of the nuclear force and of surface diffuseness [3]. In order to achieve the limiting angular momentum for a particular compound system, it is necessary to use a suitable target projectile combination, each of which will have a limiting orbital angular momentum $\ell_{f\ell}$ for fusion into a compound nucleus. In terms of the classical friction model [4-8], (see Fig.2) this arises because an incoming trajectory, shown by the thick line, has to end inside a pocket of the real potential (thin lines) if fusion is to occur. This may require both a loss of kinetic energy ΔE and of orbital angular momentum $(\ell_i - \ell_f)\hbar$. The former causes heating of the two nuclei and the latter, arising from tangential friction, involves the transfer of angular momentum to the two components. Since the centrifugal barrier becomes less with increasing projectile mass, the maximum angular momentum for which the potential has a pocket increases and hence $\ell_{f\ell}$ increases. (This does not apply for very heavy target/projectile systems because of increasing Coulomb energy.) For bombarding energies $E_{cm} \gtrsim 7$ MeV/amu there appears to be a change of reaction mechanism possibly involving projectile breakup with consequent incomplete fusion and pre-equilibrium emission [9]; deep inelastic collisions may also begin to take place. It is therefore possible that the increase in complete fusion cross section σ_{CF}, resulting from the orbital angular momentum reduction due to friction, may not occur above this energy. Estimates for $\ell_{f\ell}$ from the Bass model [4], assuming a limit of 7 MeV/amu for fusion through the friction mode, are shown in Fig.1. It is apparent that projectiles with A ≳ 28 are required to reach the limit ℓ_{II}. Projectiles in the region of $28 \lesssim A \lesssim 50$ are in any case most convenient for high angular momenta HI,xnγ studies because, for the same angular momentum, they produce lower excitation

energies than lighter particles.

Although the condition $E_f = 0$ may set a limit to how high in angular momentum we may study an equilibrated nucleus, this limit is well above that for practical study of the resultant continuum γ-rays. The reason is that, long before this limit is reached, either fission or α-decay, which removes considerable angular momentum from the system, has become the dominant mode of decay. The dot-dashed line in Fig.1 shows an estimate for the fission upper limit. From this it appears that it will not be easy to study super-deformed nuclei through γ-ray measurements. The region with $A \lesssim 110$ seems most favourable for its study. The possibility of its observation in this way may therefore depend on the occurrence of favourable shell effects.

Some of the factors relevant to two competing processes in a HI,xnγ reaction at low angular momentum are illustrated in Fig.3, which shows a level diagram for an α,2nγ reaction with rare earth nuclei. The compound nucleus A,Z formed at an excitation energy of 25 MeV can decay by neutron emission to the nucleus A-1,Z, by α-emission to A-4,Z-2, etc. and also by fission. The decay of a highly excited nucleus is thought to be governed primarily by statistical phase space considerations. Hence roughly, the relative probability for neutron and α-emission is given by the ratio of the maximum level densities in the two residual nuclei, for which the transmission coefficients for particle decay are about unity. In the case illustrated, the maximum excitation energy reached in neutron decay for this condition is about ten MeV higher than that for α-decay, in spite of the fact that in the ground state the α-particle is unbound by 2 MeV whilst the neutron has a binding energy B_n of 8 MeV. This arises because the α-particle has to surmount a large Coulomb

barrier. The large difference in excitation energy causes a corresponding large difference in level density, hence α-emission is only a few percent of neutron emission in this case. A similar result pertains to proton emission, for which $B_n = B_p$. One should however bear in mind that this result, though common, is not general. Heavy ion reactions produce neutron-deficient nuclei and, as they become more neutron deficient, B_n increases whilst B_p and B_α decrease. Eventually the probabilities for charged particle emission and for neutron emission become equal. Round about this point the HI,xnγ reaction becomes difficult to study because this competition occurs at each step in the reaction. Thus for $x = 4$ the cross section would be reduced by $\sim 2^4 = 16$. For nuclei with $A \lesssim 80$, the Coulomb barriers are lower and the binding energies change much more rapidly than for heavier nuclei as one moves away from β-stability. Hence charged particle decay is frequently the dominant mode. For clarity, I shall mainly confine the discussion to the more commonly studied HI,xnγ reaction, though most of what is said will apply also to reactions in which charged particles are emitted.

Returning now to the neutron decay sequence in Fig.3 we see that, after emission of two neutrons, most of the states formed in the nucleus A-2,Z have excitation energies below B_n for this nucleus, hence they must decay by γ-emission. Some γ-decay in competition with neutron emission also occurs as the energy rises above B_n but this soon becomes small as the neutron width Γ_n increases rapidly above threshold, becoming much greater than Γ_γ. The region where significant competition can occur depends mainly on the value of the average square matrix-element $|M_\gamma|^2$ for γ-decay. For low angular momentum this can be estimated from slow-neutron capture γ-ray data. At high angular momentum the upper boundary of the region of predominant

γ-decay, usually known as the γ-cascade region, is less precise because the excitation energy is high and neutron decay is in principle possible throughout the region (see Fig.4). The boundary of this region is usually defined as that corresponding to the probability P_γ for γ-decay, as compared with that for decay by any process, being 0.5; the lower boundary is of course the yrast line. Since neutrons can carry off very little angular momentum, the upper boundary is usually thought to be fairly sharp and to remain at about one neutron binding energy above the yrast line, unless α-decay lowers it.

At high angular momentum the situation becomes more favourable for α-emission. The reason is that the centrifugal barrier is lower for α-particles, by virtue of their greater mass, than for nucleons; they can therefore carry off angular momentum more readily. The level density dependence on excitation energy E_x is usually taken to be the same for angular momentum $J\hbar$ as for zero angular momentum, except that the zero of excitation energy is approximately that of the yrast line for $J\hbar$. Hence, lines of constant level density are roughly at constant energy above the yrast line. The arrows in Fig.4 relate to neutron decay (nearly vertical) and α-decay (sloping) leading to regions with the same level density in the residual nuclei; for simplicity we have taken the same yrast line for both though this is not a very good approximation for α-decay from lighter ($A \lesssim 100$) nuclei. It can be seen that there is a considerable energy gain for the α-particles. When this gain becomes greater than the previously mentioned energy disadvantage, α-decay may dominate over neutron emission. If we approximate the yrast line as a rotational energy corresponding to the spherical rigid body moment of inertia $J_{rig}(\text{sph})$, then the energy gain for a particle emitted with orbital angular momentum $\ell\hbar$

from a state with $J\hbar$ is

$$\Delta E(J,L) = 34A^{-5/3} [2J\ell - \ell(\ell-1)] \text{ MeV} \qquad (1)$$

The inset to Fig.4 shows values for $\Delta E(J,10)$, plotted against mass number A. It is apparent that strong α-competition with neutron decay at high angular momentum is more likely to be observed in lighter nuclei with $A \leq 120$ than in heavier nuclei.

So far we have considered emission of α-particles only in competition with neutrons. However, at high angular momentum, when the slope of the yrast line becomes steep and $\Delta E(J,L)$ sufficiently large, α-decay may become dominant in what would otherwise be the γ-cascade region near to the yrast line. This is because α-decay has now only to compete against γ-decay, for which Γ_γ is relatively small; the α-energies can be well below that of the Coulomb barrier with correspondingly low values for the transmission coefficients T_ℓ and large values of ℓ. Thus α-decay of this type can result in a termination of the γ-cascade region at high angular momentum. This effect was called "α-pinch off" in the classical papers of Grover and Gilat [10], which described the effects resulting from the statistical particle and γ-decay following HI induced reactions. If α-decay sets the high angular momentum limit to observation of γ-rays from these reactions, then α-pinch off rather than α-decay at higher excitation energy normally determines this limit. A typical termination of the γ-cascade region by α-pinch off is shown in Fig.4 (see also Fig.14).

Another high angular momentum limit to the observation of γ-rays may be set by fission. The fission saddle point has a higher deformation, and hence higher moment of inertia, than the nuclear ground state. Therefore the fission barrier $E_f(J)$, corresponding to the difference in energy between the rotating saddle point and ground

state, falls with increasing J, as illustrated in Fig.5. The variation of $E_f(J)$ can be estimated from the RLDM model [1]. Roughly speaking, when $E_f(J)$ becomes equal to B_n, the probabilities for decay by neutron emission and by fission are comparable. Since fission may compete at each step of the neutron cascade, this condition sets an approximate practical upper limit to the angular momentum for which γ-rays may be observed. Rough estimates [11] for the upper angular momentum limits set by fission and α-pinch off for representative HI,xnγ reactions are shown in Fig.6 (see also Fig.1). They suggest that fission sets the limit for $A \geq 120$ and α-pinch off for $A \leq 120$. These matters are now considered in more detail.

2. Statistical model calculations

Theoretical study of compound nucleus decay is usually made with the aid of the statistical model of nuclear reactions. In such calculations it is assumed that a compound system is formed and that successive emission of particles and γ-rays carries away the excitation energy and angular momentum. Further it is assumed that emission is independent of the mode of formation of the compound system or of preceding emissions apart from conservation of energy, angular momentum and parity. The population distribution as a function of J for the initial compound system (A,Z) formed at excitation energy E_0 is estimated from a model, or better, from experimental measurements of σ_{CF}, whilst the partial widths for particle, fission and γ-decay are evaluated from the well known expressions of the statistical model. If, for example, we are following the progress of a HI,xnγ reaction, the population distribution in the (E,J) plane of the nucleus (A-1,Z) can then be obtained. The same procedure is then repeated until, in principle, the ground state of the final nucleus of interest is reached. Clearly such a calculation is very complex and requires a large computer.

Calculations are usually carried out using a grid, typical grid spacings being 1 MeV in E and one unit in J as for example in GROGI2 [12], or by the Monte Carlo method. Most calculations do not take account of parity.

The partial width for particle decay from a state with energy E and spin J can be written as

$$\Gamma_p(E,J) = [D(E,J)/2\pi] \sum_{\text{final states}} \sum_{\ell} (2\ell+1)T_\ell \quad , \tag{2}$$

where D is the average level spacing, $2\pi\hbar/D$ the nuclear recurrence time [13] and T_ℓ the transmission coefficient for the outgoing particle with orbital angular momentum ℓ. It is usual to replace the sum over the levels of the residual nucleus by an integral over a theoretical level density expression $\rho_R(E',J')$ for the residual nucleus. The transmission coefficients are sometimes derived from optical model calculations and sometimes simplifying assumptions, such as s-wave emission, are made. Making crude assumptions about the T_ℓ we obtain for neutron emission [14],

$$\Gamma_n = (D/2\pi)(4MR^2/\hbar^2) \int_0^{E-B_n} \epsilon\, \rho_R(E-B_n-\epsilon)d\epsilon, \tag{3}$$

where ϵ is the kinetic energy of the outgoing neutron, M is the mass of the neutron and R the nuclear radius. Here and in future I have omitted explicit reference to J.

A slightly different result is obtained for decay by fission because neutron emission is three dimensional, whereas the nucleus is generally supposed to be committed to fission once it passes the saddle point, long before separation into two fragments occurs (see Fig.7). Thus fission is usually taken to be a one dimensional process though there

is no conclusive evidence for it [14]. The partial fission width therefore becomes

$$\Gamma_f = (D/2\pi) \int_0^{E-B_f} \rho_S(E-E_f-K)dK \qquad (4)$$

where K is the kinetic energy of the fission degree of freedom at the saddle. The integral is taken over the level density at the saddle point and the transmission coefficient is taken as 1 for $K \geq 0$ and zero for $K \leq 0$.

To evaluate the partial γ-ray width for statistical decay one has to take into account that the electromagnetic transition operator is a one body operator. Thus most of the lower energy states at E_f may be connected to higher states at E_i. However the reverse is not the case and only a small proportion of those with the much higher density at E_i differ from the lower states in the coordinates of one particle only. Including this, one obtains, for multipolarity λ,

$$\Gamma_\gamma(i\rightarrow f) = D\, C_{\lambda\pi}(E_i-E_f)^{2\lambda+\alpha}\, \rho(E_f) \quad , \qquad (5)$$

where π designates whether the transition is electric or magnetic. The quantity C depends on the average squared matrix element $|M(\lambda,\pi)|^2$ between states allowed by the transition selection rules and by the one body nature of the operator. In most calculations to date, α has been taken equal to unity following Blatt and Weisskopf [13]. However recently Liotta and Sorensen [15], in an improved calculation regarding the one body nature of the operator, have shown that it is more accurate to take $\alpha = 2$. It should also be noted that if one puts $|M(\lambda,\pi)|^2 = H_{\lambda\pi} M_W^2(\lambda,\pi)$, where M_W^2 is the Weisskopf single particle estimate (W.u.) and $H_{\lambda\pi}$ a hindrance factor, then $H_{\lambda\pi}$ may also depend on (E_i-E_f). Thus one might suppose that in the case of dipole radiation,

for example, H_{1E} would increase as E_i-E_f approached the energy of the giant dipole resonance. At the present time our only knowledge of $|M(\lambda,\pi)|^2$ is for dipole transitions in the region of the neutron threshold from slow-neutron capture experiments. Even these can only be measured for nuclei near the β-stability line. Generally it is thought that the cascade of statistical γ-rays consists mostly of dipole transitions. In the γ-cascade region it is frequently not sufficient to take account only of the statistical γ-rays because in deformed nuclei strongly enhanced E2 transitions (300±100 W.u.) [16] occur through collective bands roughly parallel to the yrast line. Such competition between statistical and collective transitions has only recently been included in calculations [11,15,17].

As can be seen from eqs.3-5, values obtained for the partial widths depend strongly on what is assumed for $\rho(E,J)$. Various prescriptions for these are used but at high energies above the yrast line they are frequently of the form

$$\rho(E,J) = N(2J+1)U^{-2}\exp[2(aU)^{1/2}] \quad , \qquad (6)$$

where $U \simeq E\text{-}E_{yrast}$ at high angular momenta (for low angular momenta a pairing correction must also be applied) and N is a normalization constant. The quantity a is proportional to the single particle level density g in the region of the Fermi surface and N proportional to $(g/J^3_{rig})^{1/2}$ [18]. The value of a is in the region of $A/8$ MeV^{-1}. Nearer to the yrast line there is even more uncertainty as to the appropriate expression to be used. The effect of collective levels, which increases ρ, should be included [19].

There are a number of other uncertainties connected with statistical model calculations of which I mention a few. It has been suggested [20] that the commonly used expressions for the partial widths may not be

strictly correct. At excitation energies and angular momenta higher than would be of interest for HI,xnγ reactions there is possible evidence for the breakdown of the model [21,22]. It is also possible that fission may not be a strictly one dimensional process [14]. Most calculations use the sharp cutoff model for the angular momentum dependence of the complete fusion cross section, which is not correct, but it is not yet clear what dependence should be used. Further it has been suggested [23] that the probability for thermal barrier penetration of a classically trapped trajectory (Fig.2) may be important. It is argued this may give rise to pseudo compound-nucleus-fission events, in which no equilibrated compound system is actually formed. If therefore these events are interpreted as arising from compound nucleus decay, both the complete fusion and fission cross sections will be overestimated requiring the use of artificially low fission barriers in statistical model calculations.

2.1 Competition between neutron and fission decay

Having briefly outlined present theoretical treatments and pointed out a few of the uncertainties involved, I go on to consider some more detailed aspects in a qualitative way. To do this it is convenient to use the simpler, constant temperature (T), form for the level density.

$$\rho(E) = \text{const.}\exp(E/T) \qquad (7)$$

Initially the smoothly varying properties of the RLDM are assumed.

From eqs.3 and 4 one can deduce [14] that

$$\Gamma_f/\Gamma_n \simeq [0.5K_0/TA^{2/3}] \exp[(B_n-E_f)/T] \qquad (8)$$

where $K_o \approx 10$ MeV and T is approximately proportional to $E^{1/2}$. It follows from eq.8 that:

(i) If $E_f \gg B_n$ then Γ_f/Γ_n is small and <u>increases</u> rapidly with increasing E for a given J.

(ii) If $E_f \ll B_n$ then Γ_f/Γ_n <u>decreases</u> with increasing E for a given J.

(iii) Since E_f decreases with increasing J, Γ_f/Γ_n increases rapidly with J for a given E.

These simple conclusions are fairly well born out by calculations with more realistic level densities, where the main parameters of the calculations are E_f and a_s/a_ν. (a_s and a_ν are the level density parameters at the saddle and for the nucleus following neutron emission.) An example, from the calculations of Hagelund and Jensen [24], is shown in Fig.8; here the quantity P_f is approximately $\Gamma_f/(\Gamma_f+\Gamma_n)$. It is noteworthy, that for J = 40, P_f is almost independent of excitation energy and has the value of about 0.08. This would be expected from eq.8, when $E_f \approx B_n$, a value of 0.07 being obtained when we take a typical value of 2 MeV for T at high excitation energy.

The fact that this region of roughly constant Γ_f/Γ_n occurs when Γ_f/Γ_n is still rather small may have the important consequence that fission in the <u>last stage</u> of the reaction may in some cases set the upper angular momentum limit to the γ-cascade region. This is because (a) neutrons carry off little angular momentum, so there is little change to the nuclear angular momentum distribution after each neutron emission and because subsequent nuclei usually have: (b) higher values of B_n because they are increasingly neutron deficient; (c) increasing values of the fissility parameter Z^2/A and therefore decreasing values of E_f; (d) decreasing moments of inertia

which make E_f drop more quickly with increasing J (this is probably a smaller effect than the others); (e) decreasing values of T, thus increasing Γ_f/Γ_n if $E_f \simeq B_n$. All of these considerations suggest that in a certain region of angular momentum where $E_f \simeq B_n$, Γ_f/Γ_n may increase after each neutron emission, suggesting that fission in the final nucleus, possibly even in competition with γ-decay, may set the limit to the γ-cascade band. It should be noted that these considerations probably do not apply when α-emission is the significant decay mode since for α-emission (a), (b) and (c) do not apply. That (B_n-E_f) increases with increasing neutron deficiency, due to (b) and (c), is illustrated in Fig.9. This shows J values for $E_f = B_n$, calculated from the RLDM for different nuclei. An experimental illustration is given in Fig.10 which shows the fission cross sections (σ_f) for a range of Pb compound systems induced by ions of ^{28,30}Si [25].

The conclusion above has strong experimental support from measurements of fission lifetimes with the blocking technique [26,27]; these measurements in fact stimulated the theoretical investigations [24,27]. Natural tungsten was bombarded with beams of ^{12}C, ^{16}O and ^{19}F and the results analysed in terms of two components with lifetimes $\tau >$ and $< 10^{-16}$ sec. It was found that the percentage of the long lived component, which must arise from fission occurring at relatively low energies above the yrast line, rose from small values, for bombarding energies near to the Coulomb barrier, to a maximum around 22% and then declined at still higher bombarding energies. This behaviour is illustrated in Fig.11. It can be understood qualitatively; at low bombarding energies the angular momentum is low and multiple chance fission negligible, near the maximum the first chance Γ_f/Γ_n is still small but Γ_f/Γ_n increases or remains roughly constant after each neutron emission, whilst at higher energies the angular momentum is

so high that first chance fission accounts for most of the decay probability. The calculations [22,25] reproduce the experimental data reasonably well and calculated population distributions weighted by the fission probabilities are shown in Fig.12. Also shown are contours corresponding to lifetimes of 10^{-17} and 10^{-16} sec. It would be interesting to see whether such calculations, here carried out for a different purpose, indicate that a practical upper limit to the observation of continuum γ-rays at high angular momenta is set by this phenomenon. Study of it is in any event of considerable interest since it may throw light on the problem of fission barriers at high angular momenta and differring temperatures.

2.2 Competition with γ-decay

The matrix elements for γ-decay are of crucial importance in determining both the width of the γ-cascade band in terms of energy above the yrast line and its termination at high angular momentum by α-decay or possibly by fission. Those likely to be of greatest importance are the E1 statistical and the E2 collective matrix elements. However, most calculations have only included the former. An early calculation of Gilat et al.[28], illustrated in Fig.13, shows the effect on the γ-cascade band of varying the magnitude of $|M(E1)|^2$ to which the parameter ξ_1 is proportional, $\xi_1 = 10^{-7}$ being the value determined at the neutron threshold for nearby nuclei. No collective transitions or fission decay were included in this calculation. Some authors have assumed the possibility that the transition probability for a given excitation energy above the yrast line may be proportional to $2J+1$ on the basis of a single particle model estimate for $|M(E1)|^2$ by Sperber [29]. Sometimes a $(2J+1)^2$ dependence has been assumed, on the basis of a misprint in Sperber's paper. Such a

dependence would have a great effect and, for example, the result for $\xi_1(J) = 10^{-7}(2J+1)$ is very similar to that for $\xi_1 = 10^{-5}$ in Fig.14. However this interpretation of Sperber's matrix element is erroneous, arising from a different definition of $|M|^2$ to that used in the computer codes [30].

The present situation regarding the magnitude of $|M(E1)|^2$ and its variation with J and excitation energy is very uncertain. A recent measurement by Cabot et al.[31] appears to require a tenfold increase in $|M(E1)|^2$ over the "slow neutron value" to explain the magnitude of the $^{93}Nb(^{63}Cu,1n)^{155}Yb$ cross section but the effect of collective E2 transitions was not included. The necessity to include them for many nuclei is illustrated in Fig.14. This shows estimates of the lifetimes of the statistical transitions deduced from slow neutron data, and a line where these lifetimes are equal to those of the collective transitions. For $J \gtrsim 50$ the γ-ray lifetime in most or all of the γ-ray cascade region depends on the collective and not on the statistical transitions. This is because the collective lifetime is approximately proportional to $(4J-2)^{-5}$ and has been taken to be independent of energy above the yrast line. Presumably at high nuclear temperature the collective motion will be destroyed but at present it is not entirely clear how high in energy above the yrast line it will persist. The competition between statistical and collective transitions has an effect on the relative feeding intensities of the ground state band [15,17]. Therefore, calculations, including this competition, based on experimental feeding intensities and lifetimes of the E2 yrast cascade may possibly help to throw light on the value of $|M(E1)|^2$.

2.3 Shell and other effects

One might expect shell effects to have a significant influence on

particle, fission and γ-decay. Major changes of particle levels near the Fermi surface with consequent changes of g occur as the nuclear rotational frequency ω increases [32]. Furthermore changes in nuclear shape symmetries may occur causing level density changes due to altered possibilities for collective motion [19]. Such changes in $\rho(E,J)$ may differ in the different final nuclei and may have a significant effect on relative decay probabilities. For example consider the case where a change occurs, involving collective levels above $J\hbar$ to non-collective levels, and hence decreased level density, below $J\hbar$. Here Γ_α for the yrast region would be reduced for angular momenta up to $\simeq (J+\ell)\hbar$ in the initial nucleus, as compared with what it would have been if collectivity had continued below $J\hbar$; $\ell\hbar$ is the mean angular momentum carried by the α-particle, which is approximately in the range of 10-15 $\hbar$ for decay in the yrast region. Since the γ-rays carry off relatively little angular momentum, Γ_γ would not be affected in the same way, so that $\Gamma_\alpha/\Gamma_\gamma$ would be reduced, possibly resulting in an increase in the angular momentum when "α-pinch off" occurs.

Furthermore the related changes in the energies of the minima and saddle points of the nuclear potential surfaces may cause changes in the effective particle separation energies and fission barriers. That changes of shape with consequent changes in collectivity, even for modest $J \simeq 30$, do take place is strongly suggested by continuum γ-ray measurements [33]; they seem most likely to occur in spherical or weakly deformed nuclei. Calculations of nuclear potential surfaces as functions of angular momentum have been carried out using the Strutinsky procedure [2,32,34,35]. One of the major difficulties of such calculations is to adequately parametrize the nuclear shape [2]. Further, the calculations usually refer to zero temperature and it is not entirely clear how the results are modified at realistic temperatures, though a recent attempt has been made to consider this [35].

An interesting calculation to estimate the instability, in the yrast region, of nuclei with high angular momentum to decay by neutron or proton emission has been made by Døssing et al.[36]. The instability is associated with the occupation of certain high spin orbitals. It would be interesting to extend the calculations to the more difficult case of α-emission, which seems more likely to set the limit to the termination of the γ-cascade band than nucleon emission [11].

In the case of ^{194}Hg calculated shell effects in E_f amounted to about 4 MeV, a significant change [2]. For the same nucleus calculated effective particle separation energies [35] are shown in Fig.15. These calculations, made in an attempt to explain results from the commendably complete measurements of Miller et al.[37], suggest that shell effects may significantly modify the effective separation energies and hence the relative emission probabilities. In this instance the change in behaviour of the separation energies is related to a change in shape from nearly spherical to well deformed nuclei ($\beta \simeq 0.4$) for $J \gtrsim 30$.

When such a shape change occurs, it is also necessary to take into account the change in transmission coefficients for charged particle decay. For example, in the case of α-decay in competition with γ-decay resulting in the termination of the γ-cascade band, the T_ℓ are very small and would increase markedly with increasing deformation, thus possibly terminating the band at lower J. Blann and collaborators have discussed this general question and pointed out [38-40] the dramatic effects which may occur for the super-deformed nuclei predicted by the RLDM[1]. Here, the increase in α-emission probability may be so large as to "shield" the nucleus almost completely from fission and produce evaporation residues well beyond the point where $E_f \simeq B_n$ for the compound system. The data of Britt et al.[41], shown in Fig.16, may give some support for this conclusion. This shows the maximum angular momenta ℓ_{max} for evaporation

residues, derived with the sharp cutoff approximation from measured values of σ_{ER}, and from γ-ray multiplicities. The two methods agree in the region of overlap ($E_{ex} < 120$ MeV) but the ℓ_{max} from the σ_{ER} alone appear to slowly increase above the RLDM "limit" of $\sim 65\hbar$, for $E_f = B_n$, up to $\sim 80\hbar$. On the other hand the bombarding energies corresponding to the highest values of E_{ex} are about [illegible] MeV/amu and it is possible that pre-equilibrium decay or some other process, such as massive transfer, may be causing the apparent increase in ℓ_{max}. In the absence of special shell effects, the super deformed region probably starts at angular momenta higher than those where one might easily observe continuum γ-rays. However, study of the α-particles emitted at very high angular momentum presents an exciting opportunity to extend knowledge of nuclear properties at high angular momentum beyond the region accessible to continuum γ-ray studies. Because the enhancement of Γ_α is greater when the yrast line is steeper [39,40] and from the estimates of Fig.1, it would appear that nuclei with $A \lesssim 100$ would be most favourable for observation of this effect.

3. Conclusion

So far I have mainly confined myself to an outline of the theoretical background to this subject, with only peripheral reference to experimental data. The main reason for this is that systematic data is almost non existent at present and that much of the data which has been analysed is not complete or is uncertain in some respects. For most of the questions referred to in this paper, only very detailed systematic measurements, including γ-multiplicities and spectra, cross sections for complete fusion, evaporation residue (σ_{ER}) and fission etc. as functions of angular momentum and excitation energy can give the necessary constraints on the theoretical calculations to clarify

them with any degree of certainty. Reasonably reliable techniques for measurement of some of these quantities, such as multiplicities and complete fusion cross sections have only recently been developed.

The difficulties which presently exist in the experimental and theoretical interpretation of data may be illustrated in the determination of E_f in terms of the RLDM. It has been common to parametrize $E_f(J) = B_f E_{f,RLDM}(J)$ and to determine the parameters B_f and a_s/a_ν (assumed independent of J which may be incorrect) from statistical model fits to the data. Experimentally there may be difficulties in determining σ_f and the cross section for an equilibrated compound system, which is usually deduced from the sum of σ_{ER} and σ_f. However σ_{ER} may be overestimated if pre-equilibrium emission or massive transfer occurs, whilst there may be difficulties in separating the fission component from deep-inelastic events or from events of the type described in ref. [21]. Recent statistical model calculations have given values for B_f varying from $\sim$ 0.5 - 0.65 [42-44] to $\sim$ 0.8 [44-46]. The lower values are rather surprising but it is still not entirely clear whether they arise from experimental uncertainties or deficiencies, or represent real effects. These questions have recently been discussed by Plasil and collaborators [46-47].

There are many open questions in the areas discussed here. Examples are the values and J dependence of $|M(E,\lambda)|^2$ for statistical decay, the existence of the super deformed nuclei and the effects of deformation on Γ_α, the magnitudes of E_f at high angular momenta and the effect of shell structure on all of these quantities. There is much detailed work to be done but we can surely expect answers to some of these questions in the not too distant future.

I would like to thank those who generously sent me comments and material in advance of publication. Thanks are also due to F.C. Barker and K.J. Le Couteur for comments on the manuscript.

J.O. Newton
Department of Nuclear Physics
Research School of Physical Sciences
Australian National University
PO Box 4
CANBERRA, ACT 2600, AUSTRALIA

References

1. Cohen, S., Plasil, F. and Swiatecki, W.J., Annals.Phys.(New York) 82, 557. (1974).

2. Faber, M., Polszajczak, M. and Faessler, A., Nucl.Phys. A326, 129 (1979).

3. Krappe, H.J., Nix, J.R. and Sieck, A.J., Phys.Rev. C20, 992 (1979).

4. Bass, R., Nucl.Phys. A231, 45. (1974).

5. Gross, D.H. and Kalinovski, H. Phys.Lett. 48B, 302 (1974).

6. Lefort, M., J.de Phys. 37, C5-57 (1976), and references therein.

7. Birkland, J.R., Huizenga, J.R., De J.N. and Sperber, D., Phys.Rev.Lett. 40, 1123 (1978).

8. Toncev, V.D. and Schmidt, R., Sov.J.Nucl.Phys. 27, 631 (1978); Yad.Fiz. 27, 1191 (1978).

9. Siwck-Wilczynska, K. Du Marchie Van Voorthuysen, E.H., Van Popta, J., Siemssen, R.H. and Wilczynski, J., Nucl.Phys. A330, 150 (1979).

10. Grover, J.R. and Gilat, J., Phys.Rev. 157, 802, 814, 823 (1967).

11. Newton, J.O., Lee, I.Y., Simon, R.S., Aleonard, M.M., El Masri, Y., Stephens, F.S. and Diamond, R.M., Phys.Rev.Lett. 38, 810 (1977).

12. Gilat, J., Brookhaven National Laboratory Report BNL 50246 (1970).

13. Blatt, J.M. and Weisskopf, V.M., Theoretical Nuclear Physics (Wiley) p.387, New York (1952).

14. Vandenbosch, R. and Huizenga, J.R., Nuclear Fission (Academic Press) p.228, New York (1973).

15. Liotta, R.J. and Sorensen, R.A., Nucl.Phys. A297, 162 (1978).

16. Hübal, H., Smilansky, U., Diamond, R.M., Stephens, F.S. and Herskind, B., Phys.Rev.Lett. 41, 791 (1978).

17. Nakai, M. and Faessler, A., Nucl.Phys. A307, 349 (1978).

18. Bohr, A. and Mottelson, B.R., Nuclear Structure, Vol.2, (Benjamin, New York) (1975).

19. Bjornholm, S., Bohr, A. and Mottelson, B.R. Proc. IAEA Symposium, Rochester, New York, 367 (1973).

20. Karmayan, S.A., Yad.Fys. 27, 1472 (1978); Sov.J.Nucl.Phys. 27, 775 (1978).

21. Delagrange, H., Logan, D., Rivet, M.F., Rajagopolan, M., Alexander, J.M., Zisman, M.S., Kaplan, M. and Ball, J.W., Phys.Rev.Lett. 43, 1490 (1979).

22. Logan, D., Delagrange, H., Rivet, M.F., Rajagopolan, M., Alexander, J.M., Kaplan, M., Zisman, M.S. and Duek, E., Preprint 1980.

23. Mathews, G.L. and Moretto, L.G., Phys.Lett. 87B, 331 (1979).

24. Hagelund, H. and Jensen, A.S., Physica Scripta 15, 225 (1977).

25. Hinde, D.J., Galster, W., Leigh, J.R., Newton, J.O. and Sie, S.H. (1980) to be published.

26. Andersen, J.J., Laegsgaard, E., Nielsen, K.O., Gibson, W.M., Forster, J.S., Mitchell, I.V. and Ward, D., Phys.Rev.Lett.36, 1539 (1976).

27. Andersen, J.U., Jensen, A.S., Jergensen, K., Lagsgaard, E., Nielsen, K.O., Forster, J.S., Mitchell, I.V. Ward, D., Gibson, W.M. and Cuomo, J.J., Kgl.Dan.Vid.Selsk.Mat.Fys.Medd. (1980) in press.

28. Gilat, J., Jones, E.R. and Alexander, J.M., Phys.Rev. C7, 1973 (1973).

29. Sperber, D., Nuovo Cimento 36, 1164 (1965)

30. Barker, F.C., Sperber, D., Private Communications (1980).

31. Cabot, C., Negra, S.D., Gauvin, H., Delagrange, H., Dufour, J.P. and Fleury, A., Preprint (1980).

32. Andersson, G., Larson, S.E., Leander, G., Möller, P., Nilsson, S.G., Ragnarsson, I., Åberg, S., Bengtssen, R., Dudek, J., Nerlo-Pomorska, B. and Szymanski, Z., Nucl.Phys. A268, 205 (1976).

33. Delaplanque, M.A., Lee, I.Y., Stephens, F.S., Diamond, R.M. and Aleonard, M.M., Phys.Rev.Lett. 40, 629 (1978).

34. Neergård, K., Toki, H., Ploszajczak, M. and Faessler, A., Nucl. Phys. A287, 48 (1977).

35. Faber, M. and Ploszajczak, M., Z.Phys. A291, 331 (1979).

36. Døssing, T., Frauendorf, S. and Shultz, H., Nucl.Phys. A287, 137 (1977).

37. Miller, J.M., Logan, D., Catchen, G.L., Rajagopalan, M., Alexander, J.M., Kaplan, M., Ball, J.W., Zisman, M.S. and Kowalski, L., Phys.Rev.Lett. 40, 1074 (1978).

38. Beckerman, M. and Blann, M., Phys.Rev.Lett. 42, 156 (1979).

39. Blann, M., Phys.Lett. 88B, 5 (1979).

40. Blann, M., Phys.Rev.C21, 1770 (1980); and Blann, M. and Komoto, T.T., Lawrence Livermore Laboratory Report, UCRL-83247 (1979).

41. Britt, H.C., Erkkila, B.H., Goldstone, P.D., Stokes, R.H., Back, B.B., Folkmann, F., Christensen, O., Fernandez, B., Garrett, J.D., Hagemann, G.B., Herskind, B., Hillis, D.L., Plasil, F., Ferguson, R.L., Blann, M. and Gutbrod, H.H., Phys.Rev.Lett. 39, 1458 (1977).

42. Beckerman, M. and Blann, M., Phys.Rev. C17, 1615 (1978).

43. Beckerman, M., Phys.Lett. 78B, 17 (1978).

44. Cabot, C., Gauvin, H, Le Beyec, Y., Delagrange, H., Dufour, J.P., Fleury, A., Llabrador, Y. and Alexander, J.M., Communication at International Conf. on Nuclear Behaviour at High Angular Momentum, Strasbourg (1980).

45. Gavron, A., Phys.Rev. C21, 230 (1980).

46. Plasil, F., Ferguson, R.L., Hahn, R.L., Obenshain, F.E., Pleasanton, F. and Young, G.R., (1980) to be published.

47. Plasil, F. and Ferguson, R.L., I.A.E.A. Symposium on Physics and Chemistry of Fission, Julich (1979).

Figure Captions

Fig. 1. Angular momenta as functions of mass number A. These are calculated from the RLDM [1] for representative nuclei formed in ^{40}Ar induced reactions for (a) fission instability, (b) change from oblate to triaxial shape (solid lines ℓ_{II} and ℓ_{I} respectively) and (c) equality of neutron binding energy and fission barrier height (dot-dashed line). The thin dashed lines are estimates for the maximum angular momenta for producing equilibrated compound systems with various projectiles.

Fig. 2. Classical trajectory (thick line) of an incoming projectile with orbital angular momentum $\ell_i\hbar$ trapped in the potential pocket corresponding to angular momentum $\ell_f\hbar$ after loss of kinetic energy ΔE and orbital angular momentum $(\ell_i-\ell_f)\hbar$. The potentials are shown by the thin lines.

Fig. 3. Illustration of neutron and α-decay of a compound nucleus A,Z formed at an excitation energy of 25 MeV. The Coulomb barrier for α-emission is denoted by E_{CB}, the B's are the appropriate binding energies, and the E_x denote the maximum excitation energies.

Fig. 4. Diagram showing (a) the γ-cascade region between the yrast line (lower line) and the line $P_\gamma = 0.5$, (b) the decay energies for neutron emission, with $\ell = 2$, and α-emission, with $\ell = 10$, from a state with $J = 50$ to regions with the same level density (the vertical lines correspond to B_n and B_α), (c) the energy gain $\Delta E(J,\ell)$ (see text) for this case and, in the inset, for three values of J as a function of A.

Fig. 5. Fission barrier as a function of J, calculated from the RLDM.

Fig. 6. Estimates of maximum angular momenta for the γ-cascade band [11] set by α-emission (solid lines) and fission (dashed line). Alpha-emission was taken to be in competition with collective rotational transitions, D being the level density near to the yrast line. The points are experimental measurements.

Fig. 7. Schematic diagram of nuclear potential energy as a function of deformation. Nuclear shapes at the saddle and scission points are indicated.

Fig. 8. Calculated probabilities for decay by fission of ^{196}Pb for various angular momenta as functions of excitation energy [24].

Fig. 9. Limiting angular momenta, deduced from the RLDM for the condition $E_f = B_n$, for various isotopes as a function of A.

Fig.10. Preliminary data for the total fission cross sections for $^{194-200}$Pb induced by ^{28,30}Si ions [25].

Fig.11 The percentage of a long-lived component in the fission induced by ^{12}C, ^{16}O and ^{19}F on W as a function of bombarding energy [27]. Results were obtained from two component fits to blocking dips at forward and backward angles.

Fig.12 Calculated contours of population distributions, weighted with fission probability, in excitation energy and spin for fission induced by 97 MeV ^{16}O on ^{182}W [27]. The curves centred at different excitation energies correspond to successive nuclei resulting from the ^{198}Pb compound system, formed at 62 MeV, after emission of one to five neutrons. The dashed lines are for constant lifetimes of $10^{-17}$and 10^{-16}s for ^{194}Pb. The dot-dashed curve is the yrast line. The top curve shows the fission probability as a function of spin, weighted by the triangular entrance angular momentum distribution. Values are in units of $10^{-4}\hbar^{-1}$ and the numbers on the contours are in units of $10^{-4}\hbar^{-1}$ MeV^{-1}. The inset at the top shows the calculated percentage fission yield as a function of lifetime τ. The total yield is 100% but only the components with $\tau > 10^{-18}$s are shown.

Fig.13. Calculated boundaries ($P_\gamma = 0.5$) of the yrast cascade band for various values of the parameter ξ, the "slow neutron capture value" is 10^{-7} [28].

Fig.14. Estimated lifetimes (light dashed lines) for statistical E1 γ-rays (neutron capture normalization $\simeq 1.5.10^{-2}$ Weisskopf units) are shown as functions of excitation energy and J. The heavy dashed line indicates where the lifetimes for statistical decay and for collective E2 transitions (150 W.u.) are equal. Note that the collective transitions may be more [16] or less enhanced than assumed here and that $|M(E1)|^2$ is probably not known to within at least a factor of ten. Thus the position of the heavy dashed line might vary, either up or down from that shown here. The solid lines show the yrast line and a line one neutron binding energy above it, indicating roughly the upper limit of the γ-cascade band.

Fig.15. Separation energies for protons, neutrons and α-particles as a function of the total angular momentum of $^{194}_{80}Hg_{114}$ for different angular momenta of emitted particles [35].

Fig.16. Plot of ℓ_{max} as a function of the excitation energy of the compound nucleus for evaporation residues formed by ^{40}Ar bombardments of ^{109}Ag, ^{121}Sb and $^{122,124}Sn$, and by $^{84,86}Kr$ bombardments of ^{65}Cu and $^{70,74,76}Ge$ [41]. Data are from γ-ray multiplicity measurements and measurements of the yields and A,Z of evaporation residues. The angular momentum for which E_f[RLDM] = B_n for ^{162}Er is indicated.

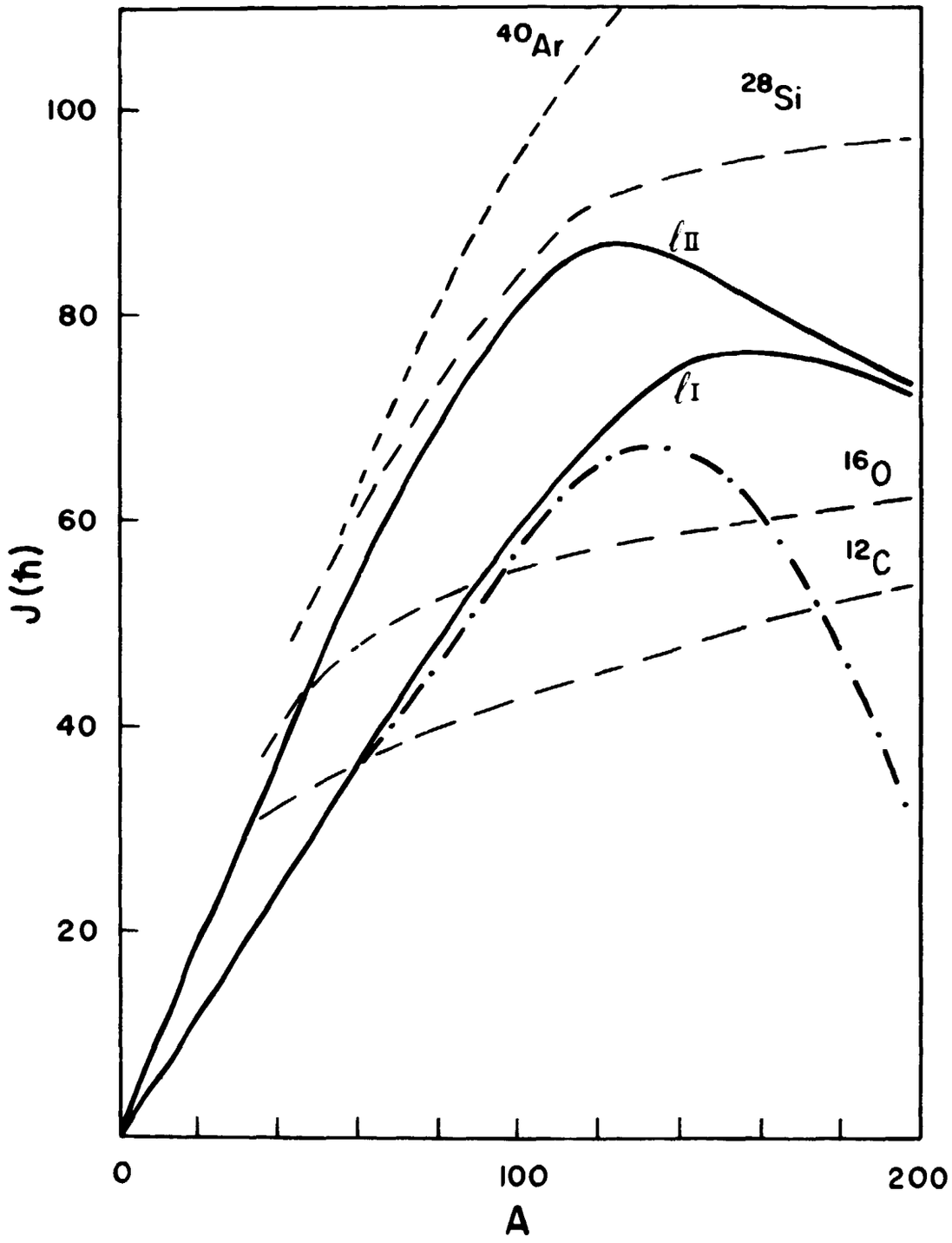
^{40}Ar
^{28}Si
ℓ_{II}
ℓ_I
^{16}O
^{12}C
100
80
60
40
20
J(ħ)
0
100
200
A

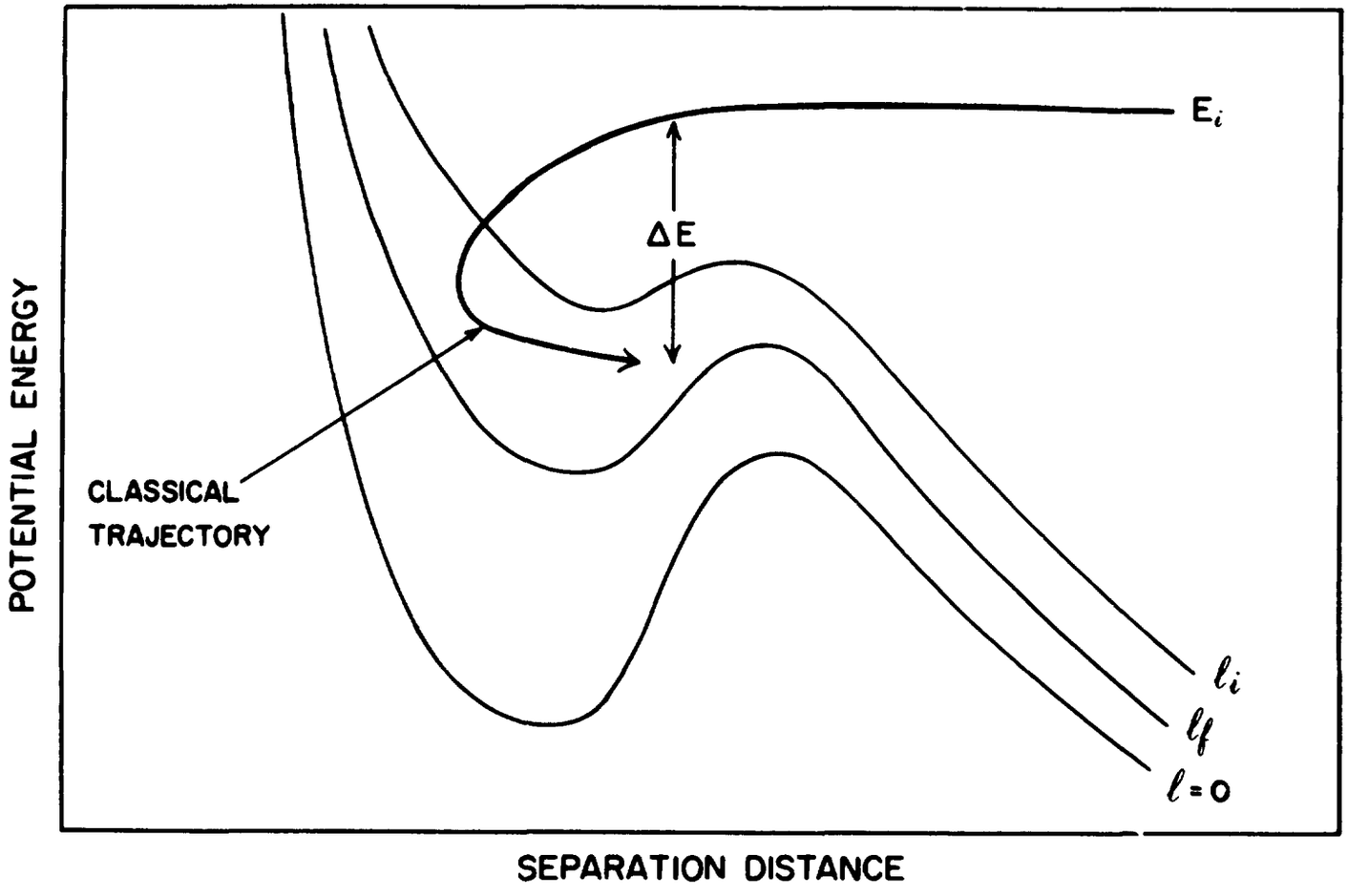
POTENTIAL ENERGY
E_i
ΔE
CLASSICAL
TRAJECTORY
ℓ_i
ℓ_f
$\ell = 0$
SEPARATION DISTANCE

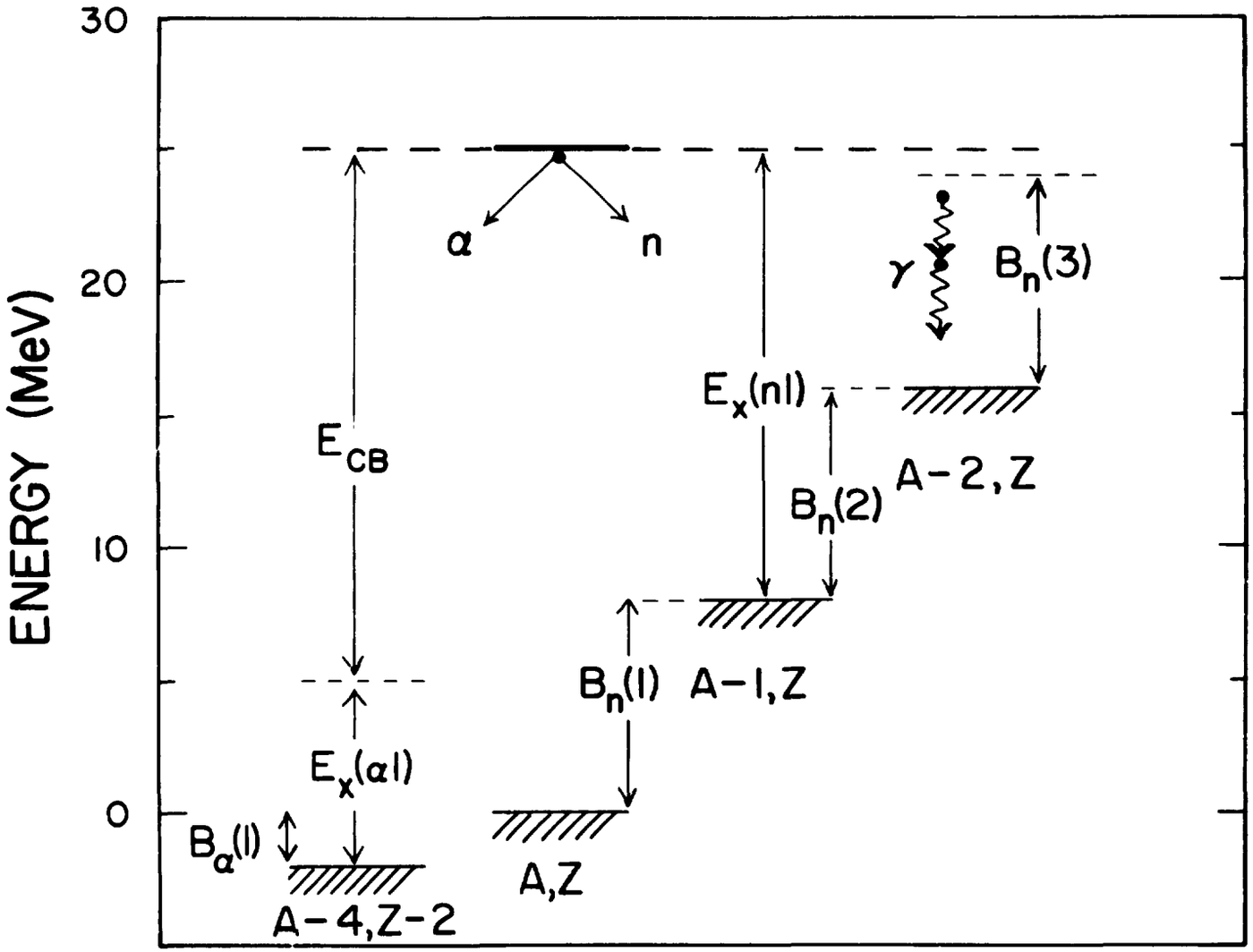
ENERGY (MeV)
30
20
10
0
α
n
γ
$B_n(3)$
$E_x(nl)$
E_{CB}
$B_n(2)$
A-2, Z
$B_n(1)$ A-1, Z
$E_x(\alpha l)$
$B_\alpha(l)$
A, Z
A-4, Z-2

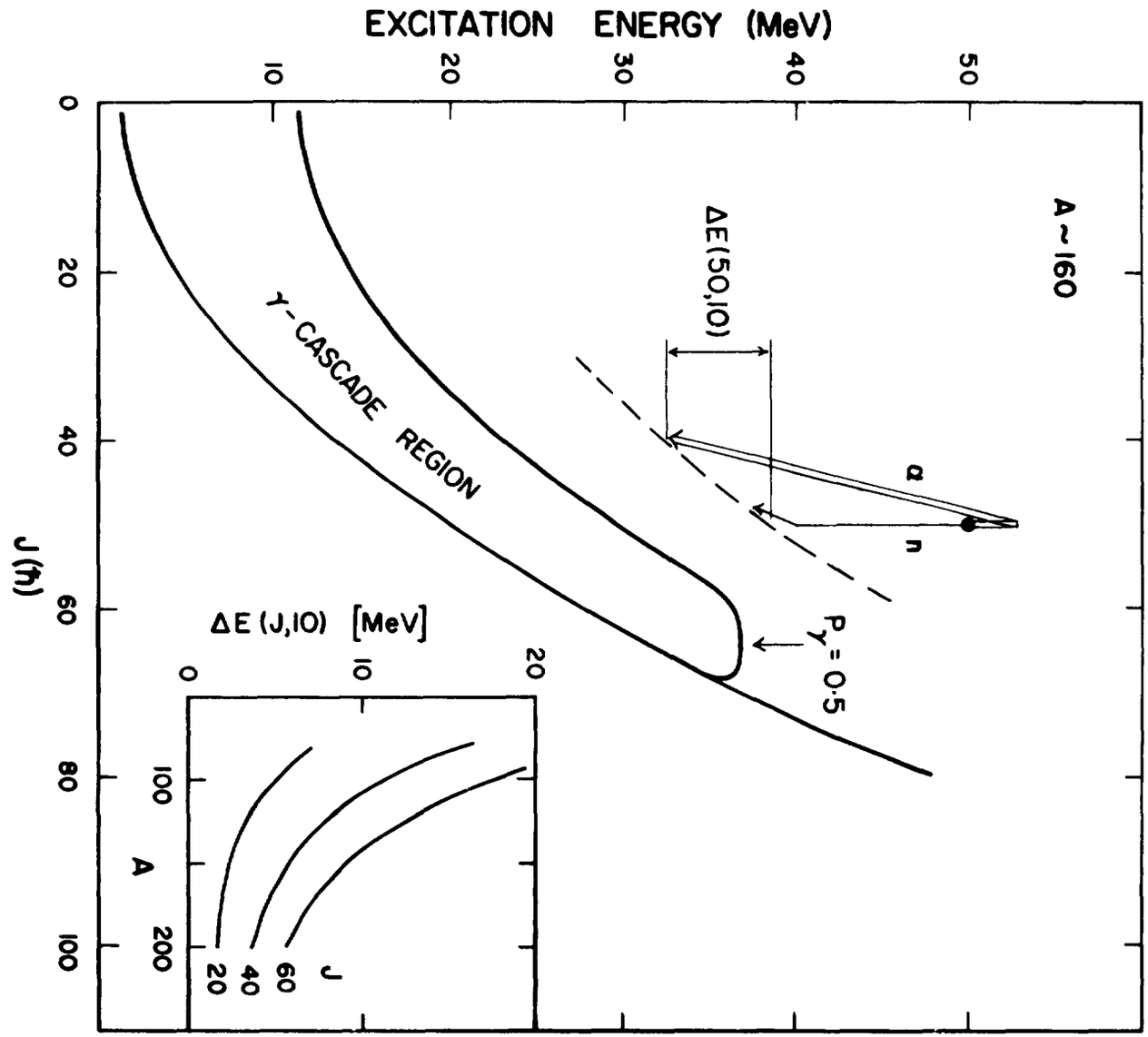
EXCITATION ENERGY (MeV)
10
20
30
40
50
0
20
40
60
80
100
J (ħ)
A ~ 160
ΔE(50,10)
γ-CASCADE REGION
α
n
$P_\gamma = 0.5$
ΔE (J,10) [MeV]
0
10
20
100
A
200
20
40
60
J

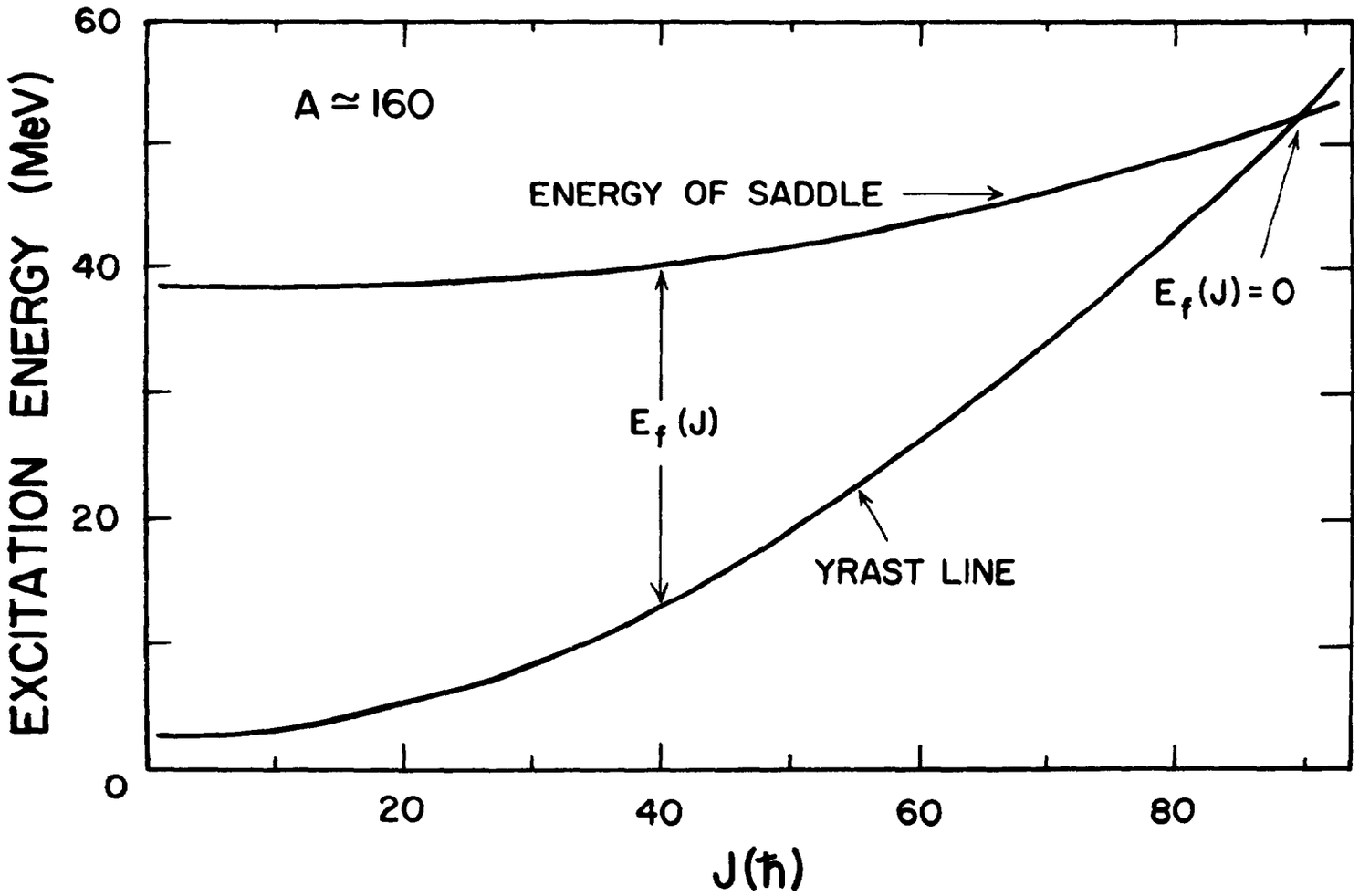
A ≃ 160
ENERGY OF SADDLE
$E_f(J) = 0$
$E_f(J)$
YRAST LINE
EXCITATION ENERGY (MeV)
J(ħ)
0
20
40
60
20
40
60
80

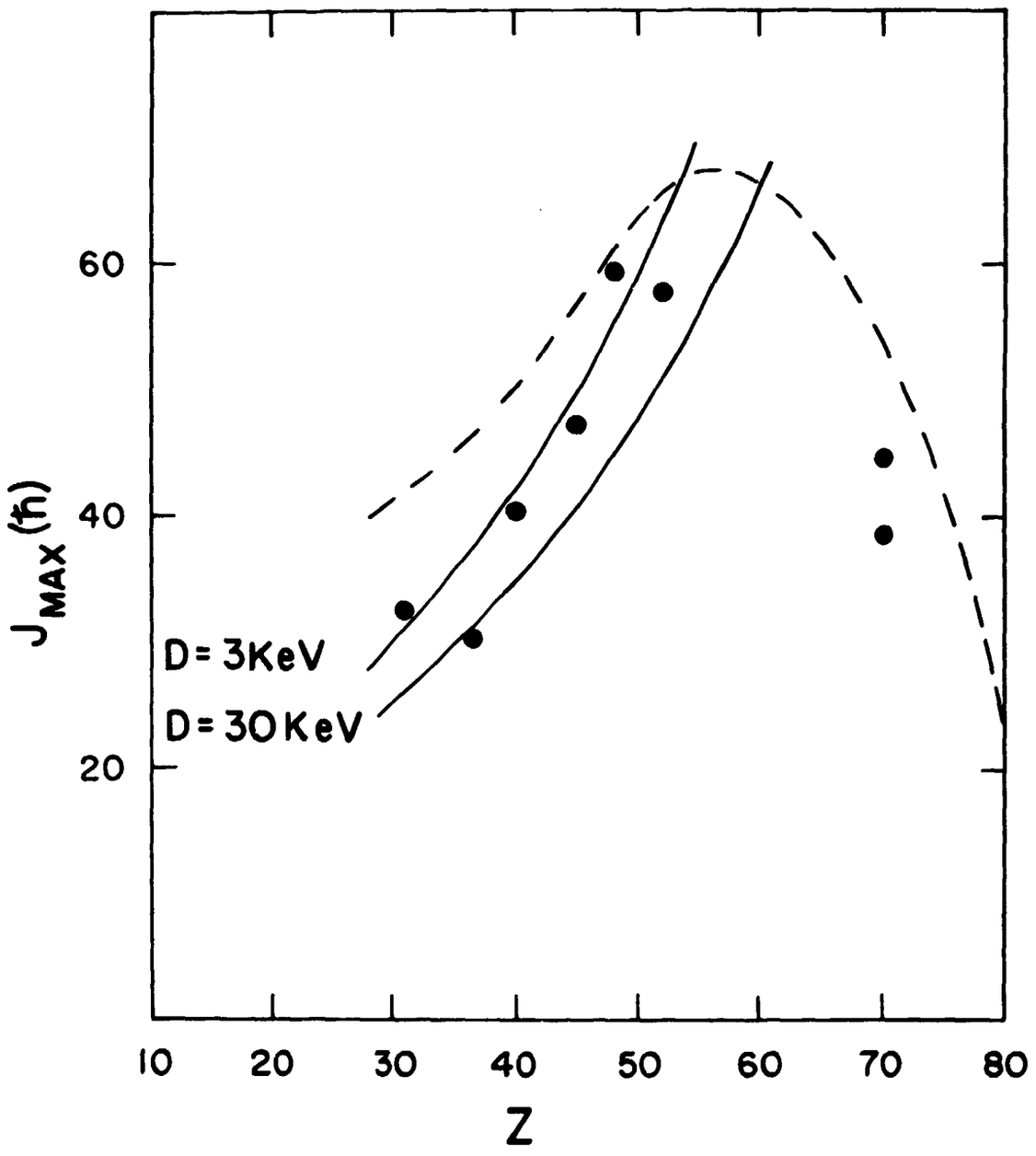
60
40
20
$J_{MAX}(\hbar)$
D= 3KeV
D= 30KeV
10
20
30
40
50
60
70
80
Z

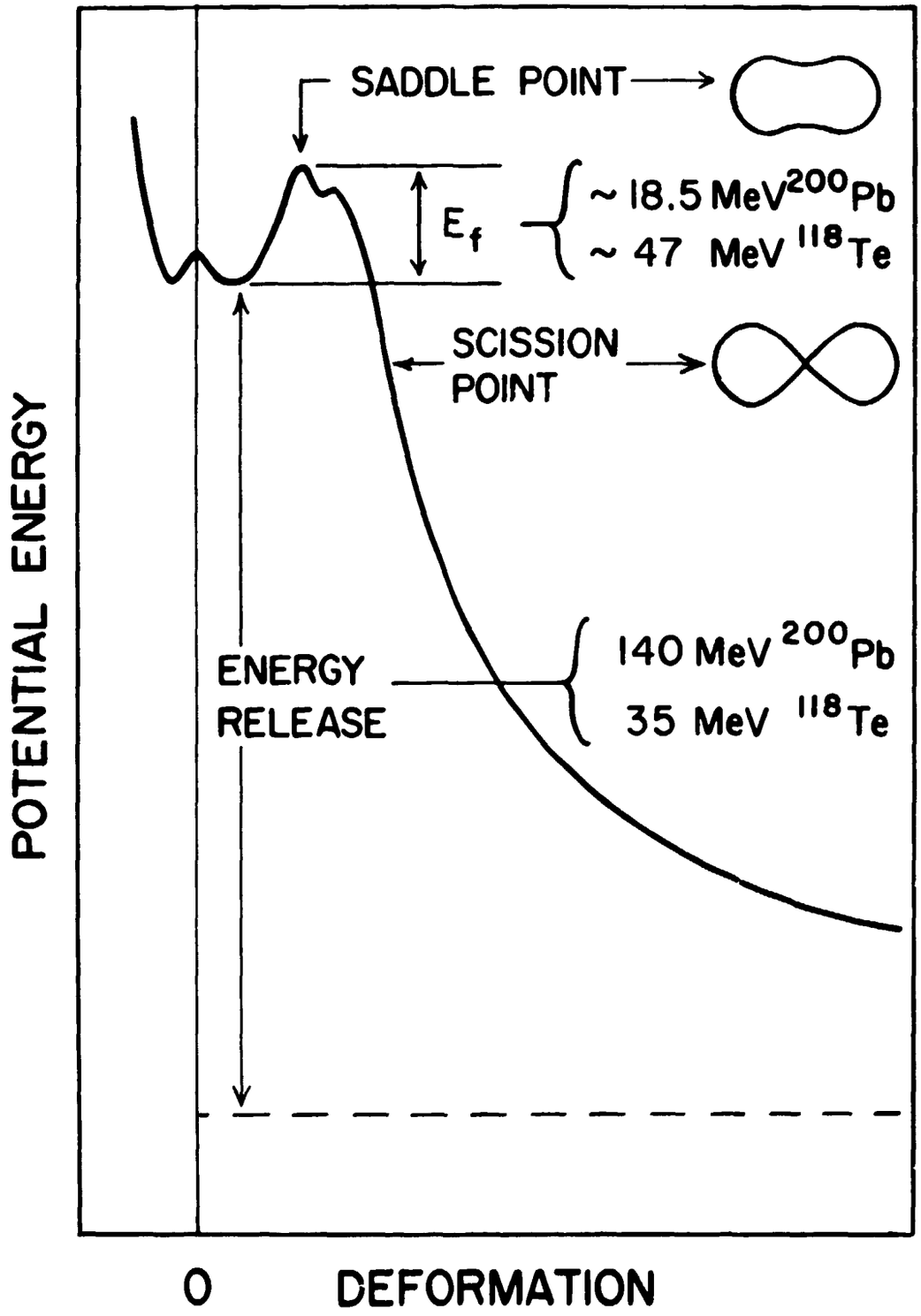
SADDLE POINT
E_f
~ 18.5 MeV ^{200}Pb
~ 47 MeV ^{118}Te
SCISSION POINT
ENERGY RELEASE
140 MeV ^{200}Pb
35 MeV ^{118}Te
POTENTIAL ENERGY
0
DEFORMATION

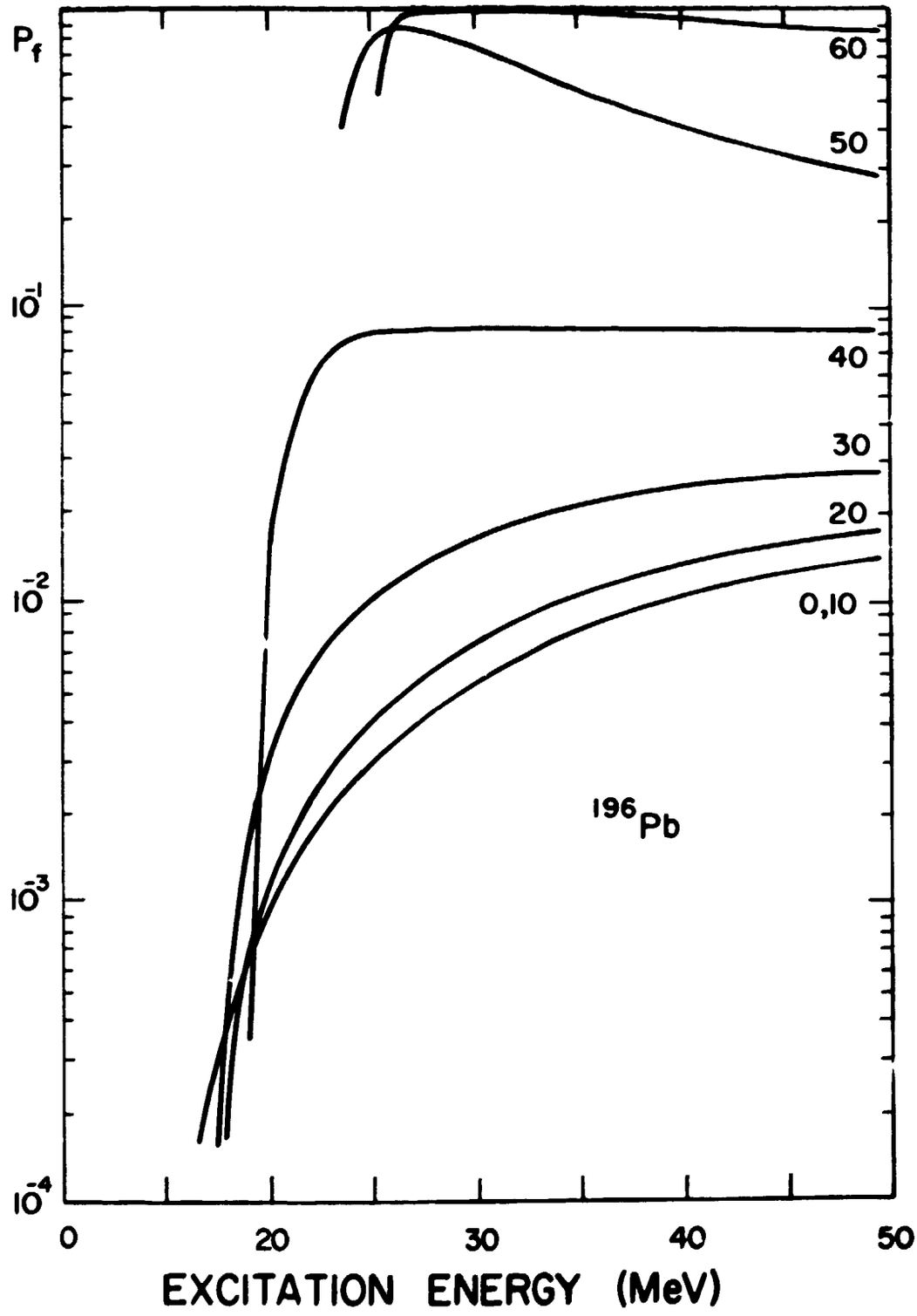
P_f
10^{-1}
10^{-2}
10^{-3}
10^{-4}
60
50
40
30
20
0,10
^{196}Pb
0
20
30
40
50
EXCITATION ENERGY (MeV)

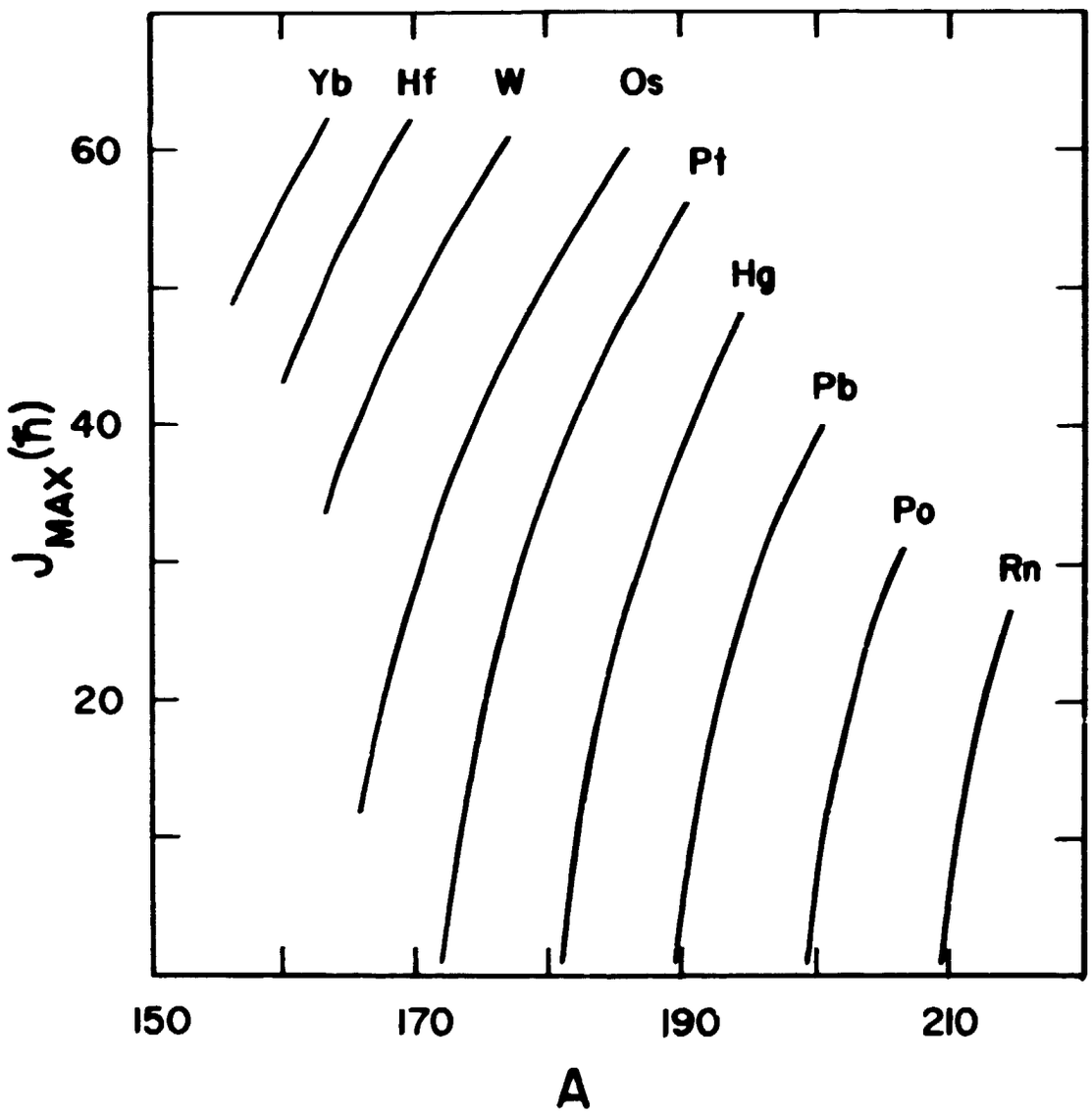
Yb
Hf
W
Os
Pt
Hg
Pb
Po
Rn
60
40
20
$J_{MAX}(\hbar)$
150
170
190
210
A

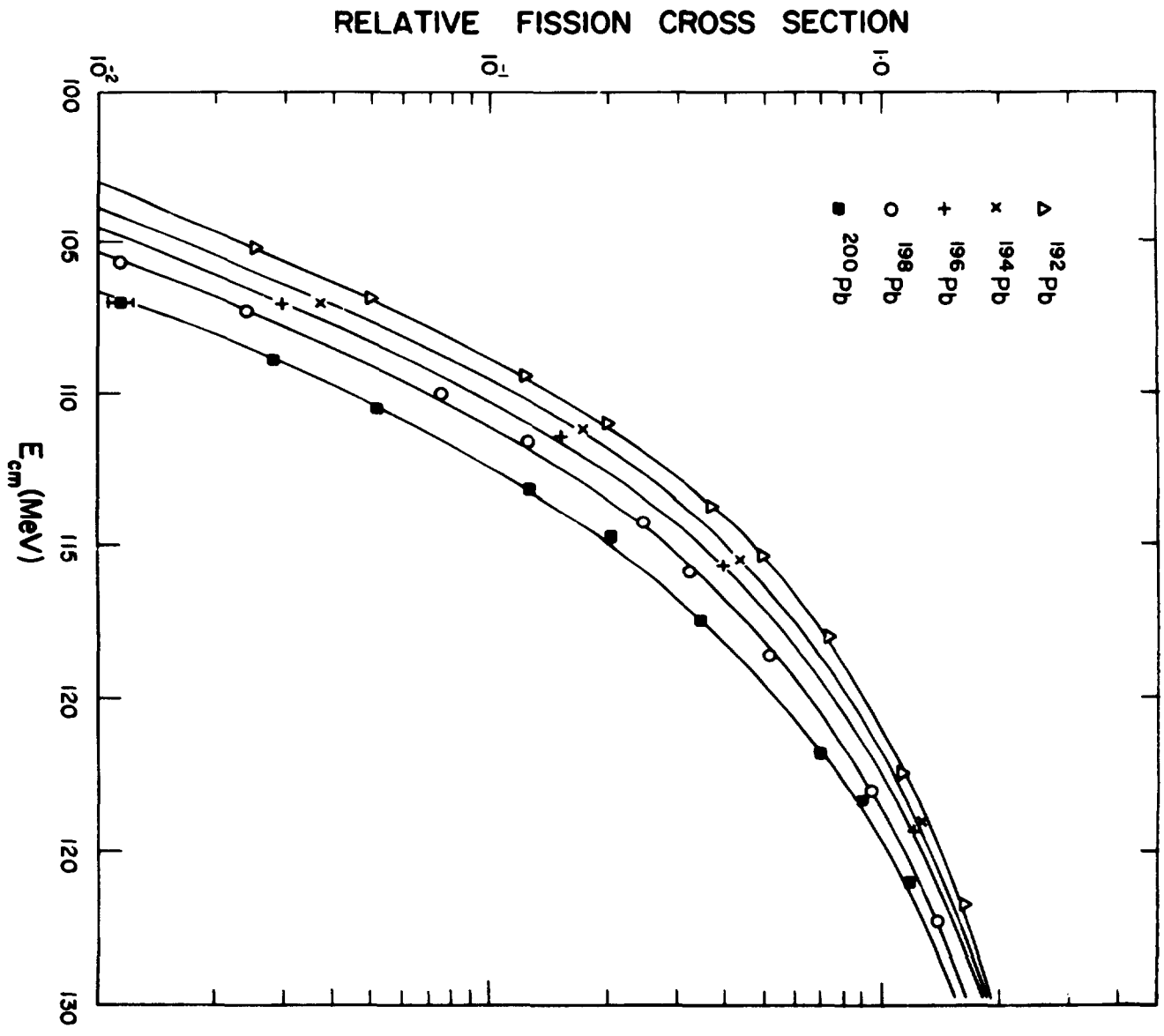
RELATIVE FISSION CROSS SECTION
10^{-2}
10^{-1}
1·0
100
105
110
115
120
120
130
E_{cm}(MeV)
△ 192Pb
× 194Pb
+ 196Pb
○ 198Pb
■ 200Pb

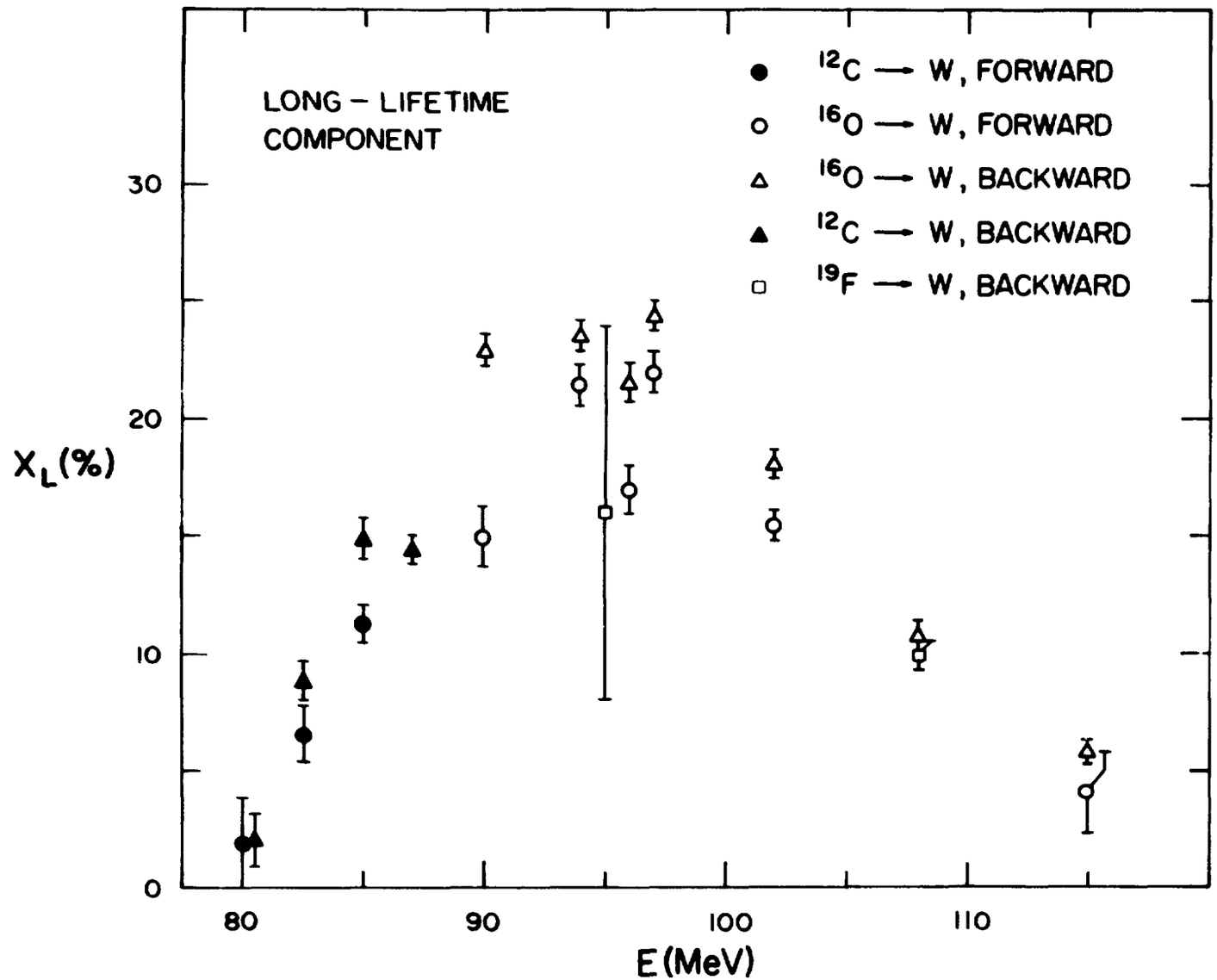
LONG – LIFETIME
COMPONENT
$^{12}C \rightarrow W$, FORWARD
$^{16}O \rightarrow W$, FORWARD
$^{16}O \rightarrow W$, BACKWARD
$^{12}C \rightarrow W$, BACKWARD
$^{19}F \rightarrow W$, BACKWARD
$X_L(\%)$
0
10
20
30
80
90
100
110
E(MeV)

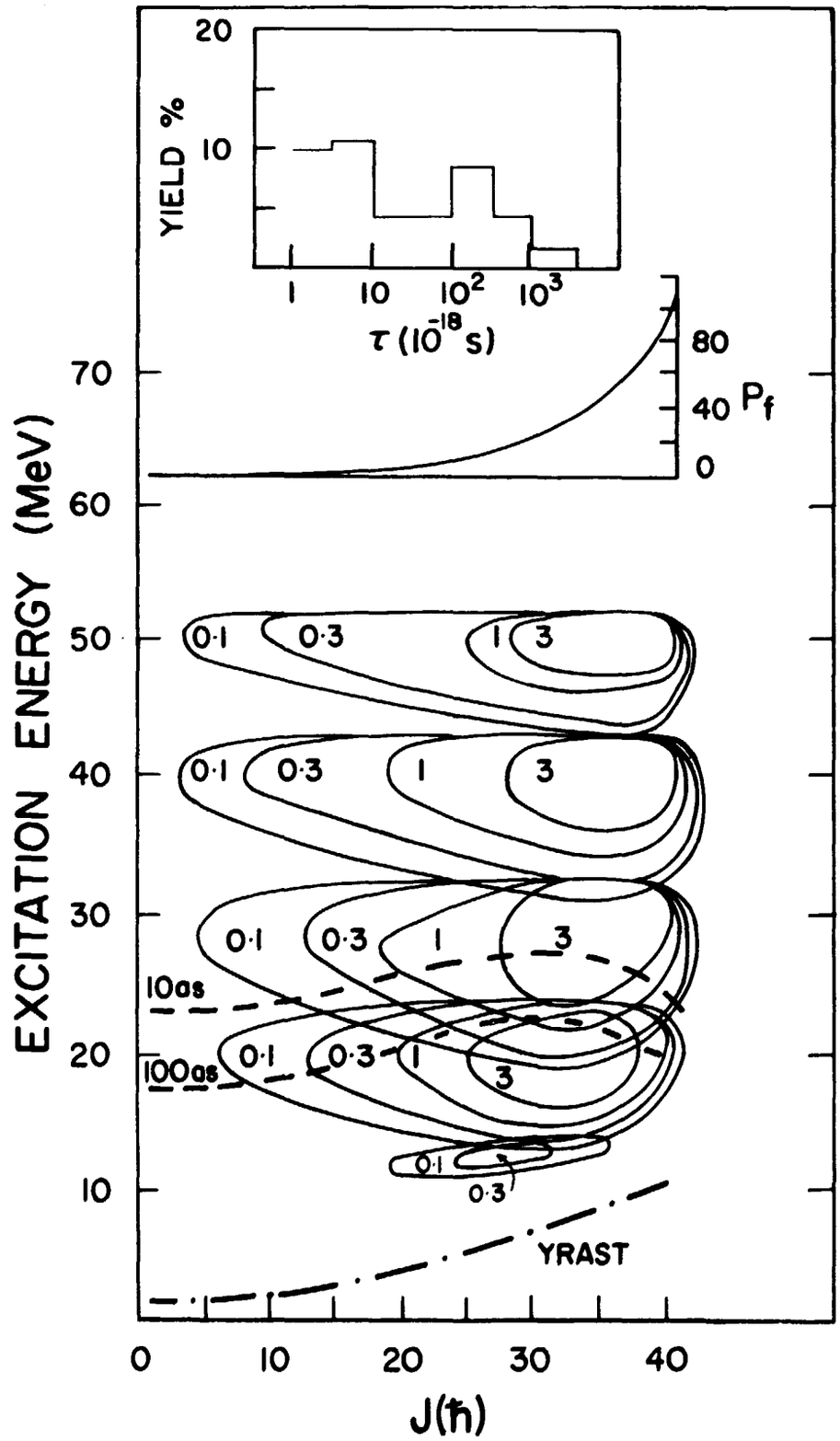
20
YIELD %
10
1
10
10²
10³
τ (10⁻¹⁸ s)
80
40 Pf
0
70
60
50
40
30
20
10
EXCITATION ENERGY (MeV)
0·1
0·3
1
3
10as
100as
YRAST
0
10
20
30
40
J(ħ)

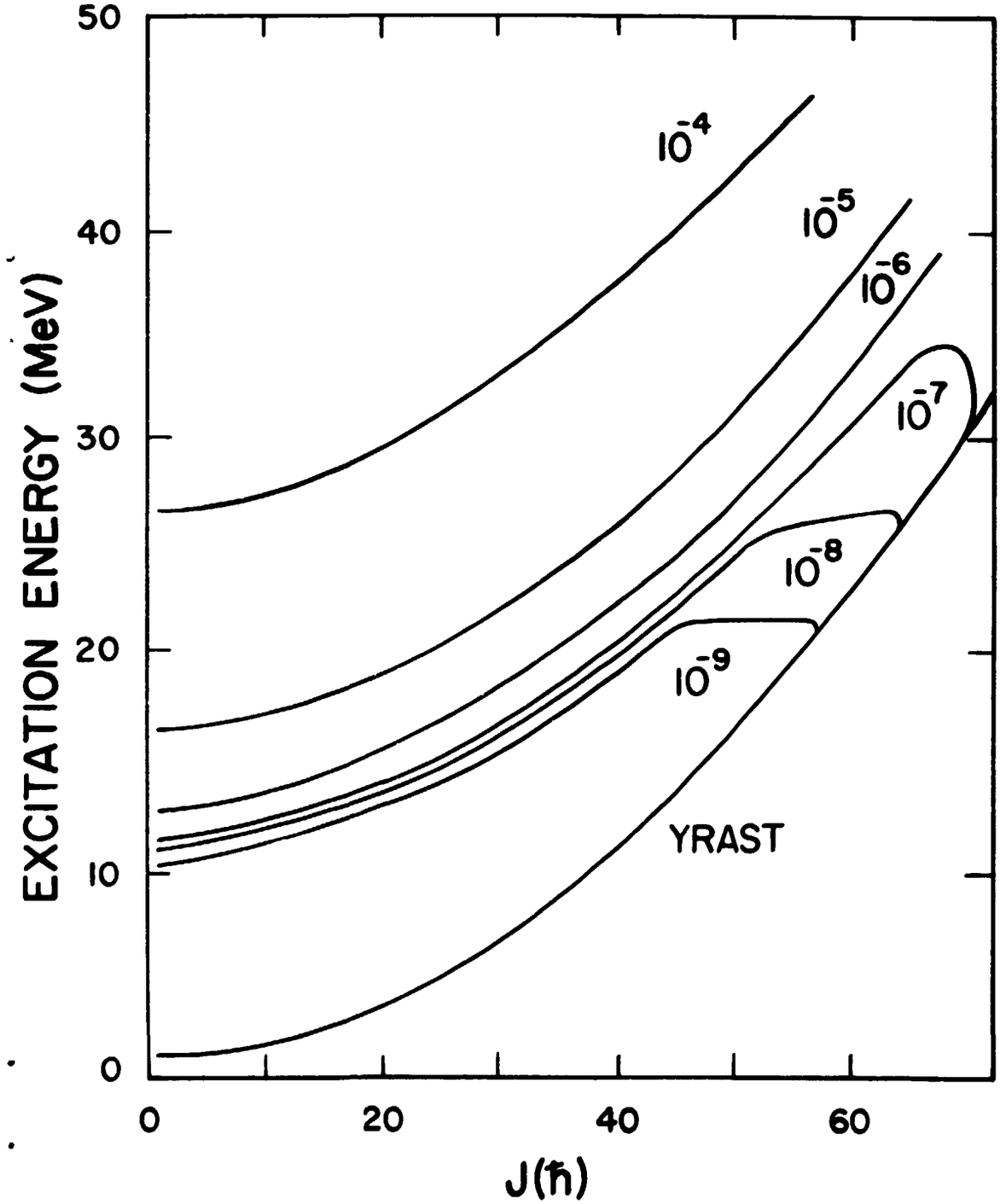
50
40
30
20
10
0
EXCITATION ENERGY (MeV)
0
20
40
60
J(ħ)
10^-4
10^-5
10^-6
10^-7
10^-8
10^-9
YRAST

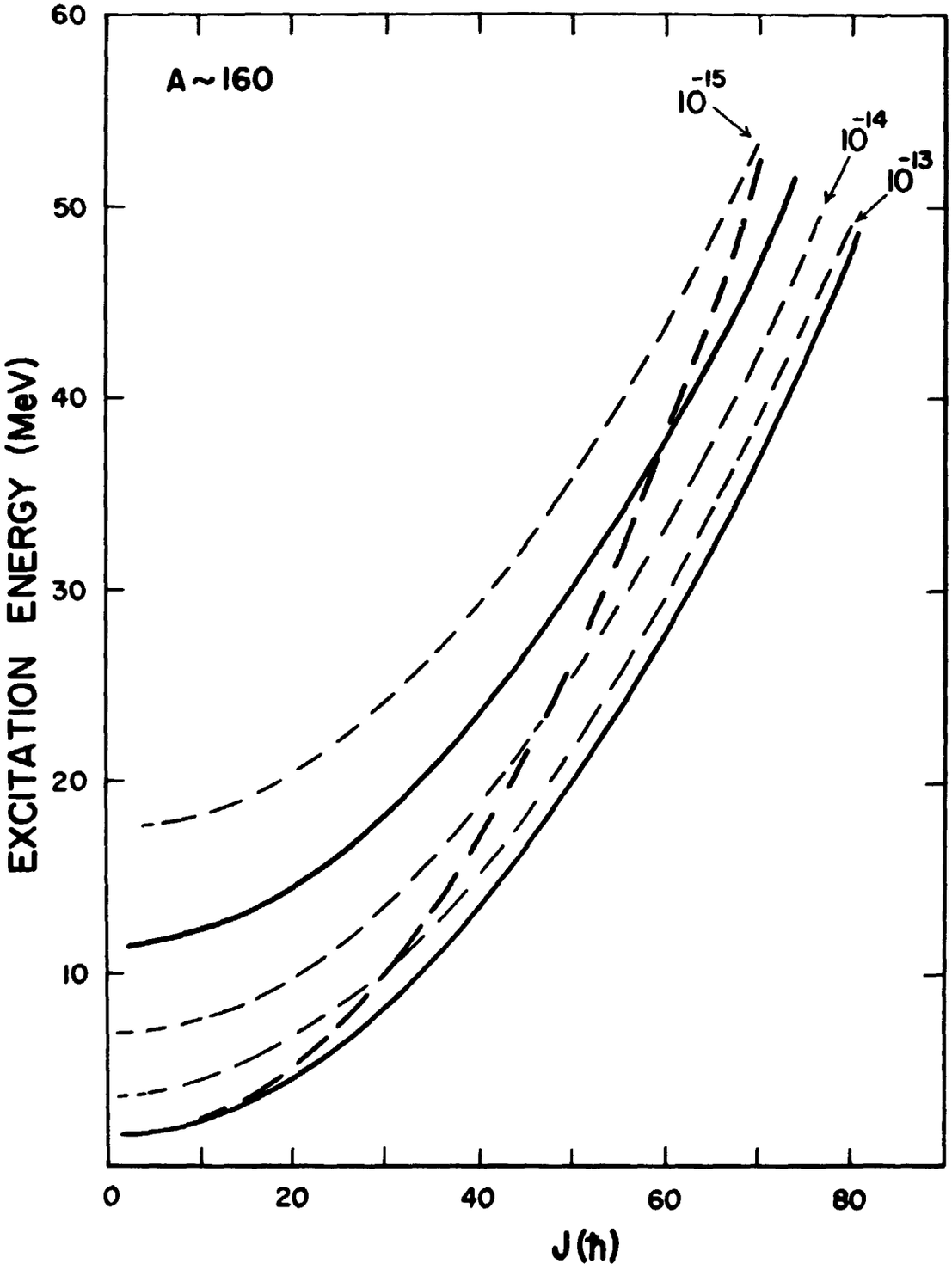
A ~ 160
10^{-15}
10^{-14}
10^{-13}
EXCITATION ENERGY (MeV)
60
50
40
30
20
10
0
20
40
60
80
J(ħ)

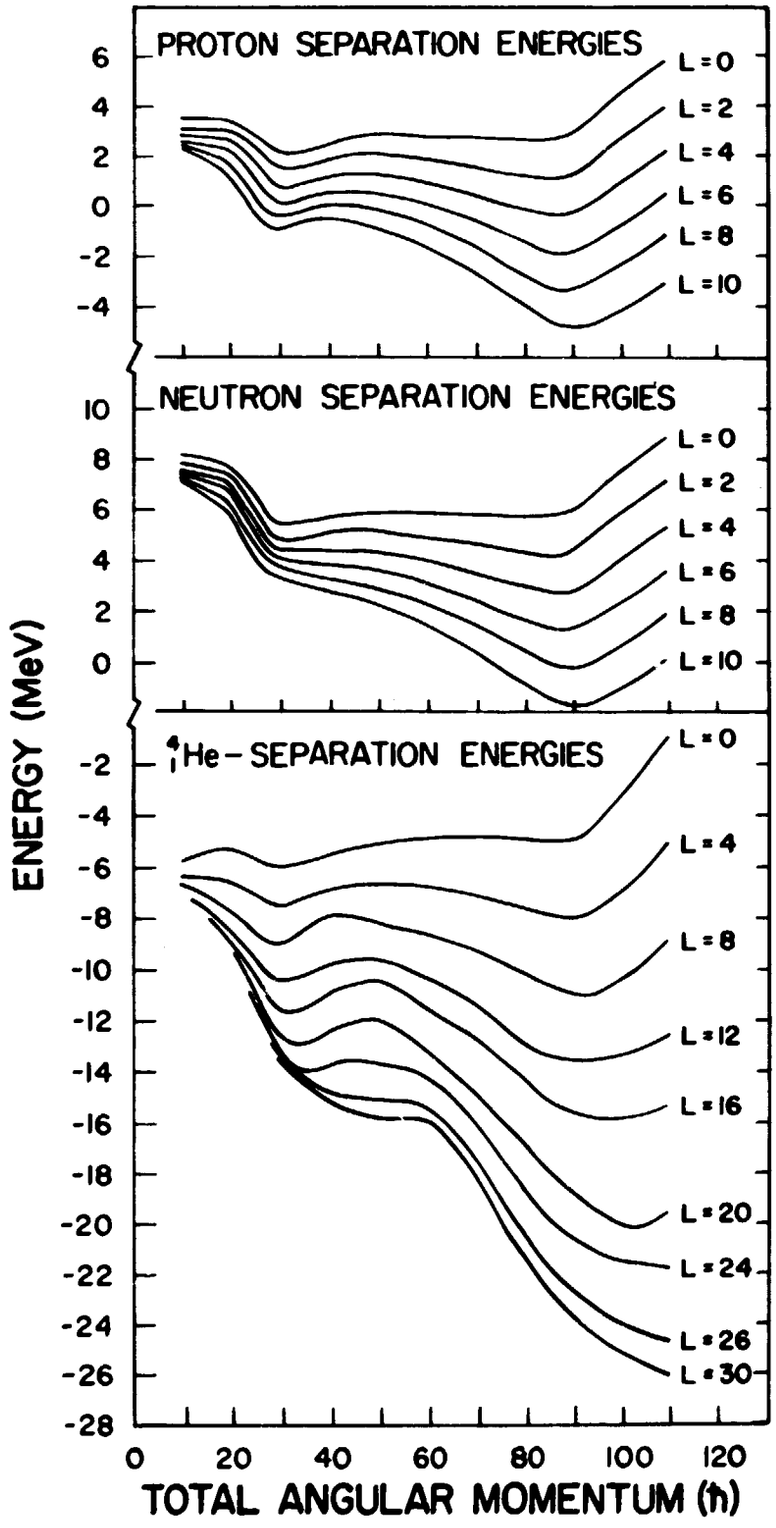
PROTON SEPARATION ENERGIES
L=0
L=2
L=4
L=6
L=8
L=10
NEUTRON SEPARATION ENERGIES
L=0
L=2
L=4
L=6
L=8
L=10
⁴₁He - SEPARATION ENERGIES
L=0
L=4
L=8
L=12
L=16
L=20
L=24
L=26
L=30
ENERGY (MeV)
TOTAL ANGULAR MOMENTUM (ħ)

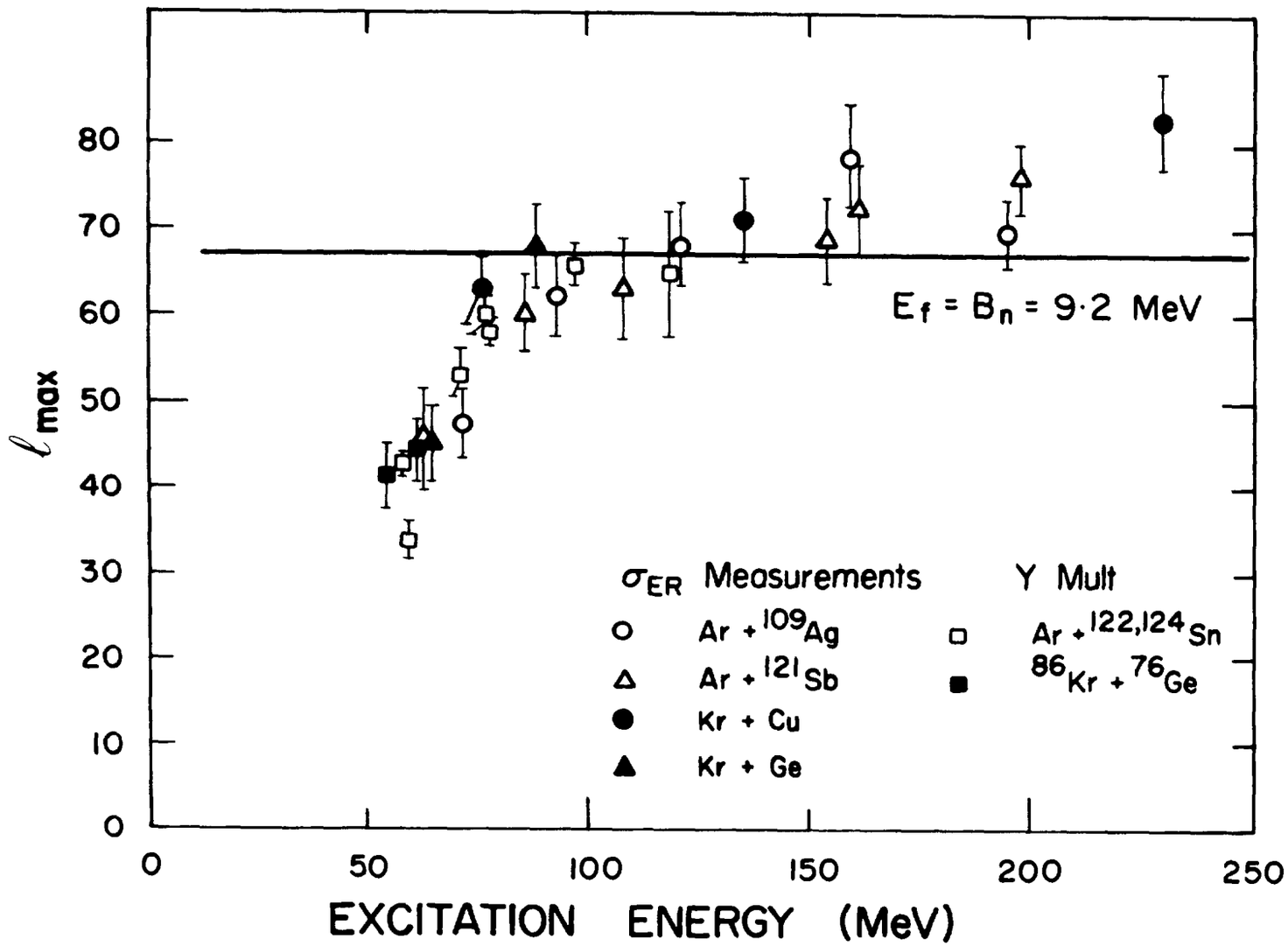
80
70
60
50
40
30
20
10
0
ℓ_{max}
0
50
100
150
200
250
EXCITATION ENERGY (MeV)
$E_f = B_n = 9{\cdot}2$ MeV
σ_{ER} Measurements
Ar + ^{109}Ag
Ar + ^{121}Sb
Kr + Cu
Kr + Ge
Y Mult
Ar + ^{122,124}Sn
^{86}Kr + ^{76}Ge